Åbo Akademi University

Helka Juvonen

Protein Adsorption and Cell Adhesion to Nanostructured Paper Coatings

Laboratory of Physical Chemistry
Center for Functional Materials
Faculty of Science and Engineering

PROTEIN ADSORPTION AND CELL ADHESION TO NANOSTRUCTURED PAPER COATINGS

Helka Juvonen

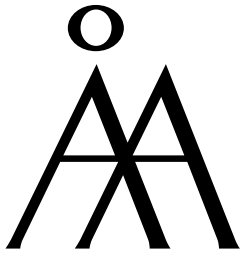

Laboratory of Physical Chemistry

Åbo Akademi University
Turku, Finland
2016

Supervised by

Professor Jouko Peltonen
Laboratory of Physical Chemistry
Åbo Akademi University, Turku, Finland

and

Adjunct professor Petri Ihalainen
Laboratory of Physical Chemistry
Åbo Akademi University, Turku, Finland

Reviewed by

Associate professor Monika Österberg
Department of Forest Products Technology
Aalto University, Helsinki, Finland

and

Adjunct professor Vesa Hytönen
BioMediTech
University of Tampere, Tampere, Finland

Opponent

Associate professor Monika Österberg
Department of Forest Products Technology
Aalto University, Helsinki, Finland

ISBN 978-952-12-3476-7 (Print)
ISBN 978-952-12-3477-4 (PDF)
Painosalama Oy – Turku, Finland

Contents

Abstract iii

Svensk sammanfattning iv

Publications v

Supporting publications v

Contribution of the author vi

1. INTRODUCTION 1

2. OBJECTIVES 3

3. SURFACE PROPERTIES 4

3.1. Surface topography 4

3.2. Wetting and surface energy 6

4. IMMOBILIZATION OF PROTEINS AND CELLS 9

4.1. Non-covalent interactions 10

4.2. Protein adsorption 12

4.2.1. (Strept)avidin 17

4.2.2. Albumin 17

4.2.3. Fibronectin 18

4.3. Cell adhesion 18

4.3.1. ARPE-19 cells 20

4.3.2. HepG2 cells 20

4.3.3. *S. aureus* bacterial cells 20

5. MATERIALS AND METHODS 21

5.1. Substrates 21

5.1.1. Latex coatings and their substrates 21

5.1.2. Pigment coatings 22

5.1.3. Paper-based test arrays 23

5.1.4. Plasma- and poly-L-lysine treated polystyrene 23

5.2. Protein immobilization 24

5.2.1. (Strept)avidin adsorption 24

5.2.2. Serum albumin adsorption 25
5.2.3. Fibronectin adsorption 25
5.3. Cell experiments....25
5.3.1. ARPE-19 and HepG2 25
5.3.2. *S. aureus* 27
5.4. Surface characterization methods....28
5.4.1. Atomic force microscopy 28
5.4.2. Contact angle measurements 31
5.4.3. X-ray photoelectron spectroscopy 32
5.4.4. Quartz crystal microbalance 32
6. SUMMARY OF THE RESULTS....34
6.1. Surface properties of the studied substrates....34
6.1.1. Composition of pristine and IR treated latex coatings 35
6.1.2. Influence of the latex blend composition on surface topography .40
6.1.3. Surface properties of pigment coatings....43
6.1.4. Surface properties of the P-PLL-PS slides 45
6.2. Protein adsorption on the latex coatings....46
6.2.1. Influence of surface chemistry and topography on protein immobilization 46
6.2.2. Activity of immobilized strept(avidin) 51
6.3. Cell study platforms....53
6.3.1. Epithelial cell growth and printability....53
6.3.2. Bacterial adhesion....57
7. CONCLUSIONS AND OUTLOOK 59
8. ACKNOWLEDGEMENTS 62
REFERENCES....63
ORIGINAL PUBLICATIONS .... **Error! Bookmark not defined.**

Abstract

Protein coatings can be prepared in order to take advantage of their biological functions such as specific binding properties and the ability to enhance or reduce cellular adhesion. The physicochemical surface properties of the substrate have an impact on the protein adsorption and its activity. The activity of adsorbed proteins plays a central role in methods based on the biochemical immobilization used in numerous bioanalytical applications.

Controlling the cell-substrate interactions is important in e.g. the development of medical devices and platforms for the cytotoxicity assays and biofilm studies. Cell studies are conventionally performed on rigid substrates. As a flexible and porous substrate, paper is an interesting alternative to the conventional materials. The surface properties of paper can be modified by various surface treatments and paper is also well suited for printing of functional materials.

The aim of this work was to develop a paper-based test platform for biochemical and biological assays by modifying the surface properties of the latex or pigment coated paper substrates. The latex coatings were treated by short-wave IR irradiation and by changing the composition of the binary latex coatings. The surface properties of the coatings and adsorption of proteins were studied. On the IR treated latex, a bimodal height distribution of hydrophobic polystyrene (PS) and hydrophilic carboxylated acrylonitrile butadiene styrene copolymer (ABS) was formed. Adsorption of proteins to the two-component latex surface resulted in a patterned structure. Adsorption of avidin to the ABS phase was found to enable a better specific binding activity to biotin.

The cell growth of ARPE-19, HepG2 and *Staphylococcus aureus* on paper substrates with different surface characteristics was studied and printability of viable cells was tested. The latex coatings were found to support the cell growth. Pre-adsorbed avidin inhibited bacterial adhesion on two-component latex.

Svensk sammanfattning

Proteinytskikt kan skapas för att utnyttja proteinernas biologiska funktioner, till exempel specifika bindningar och förmågan att hindra eller förbättra adhesion av celler. Substratets fysikalisk-kemiska egenskaper påverkar adsorptionsprocessen och aktiviteten av ytbundna proteiner. De adsorberade proteinernas aktivitet är central i metoder som baserar sig på biokemisk immobilisation, vilken används i flera bioanalytiska applikationer.

Det är viktigt att kontrollera interaktionerna mellan cellerna och substratets yta, till exempel i utveckling av medicinska apparater, cellgiftsanalyser och plattformar för biofilmstudier. Styva material, som glas och polystyrenskivor, används vanligtvis som cellstudieplattformar. Det böjbara och porösa pappret är ett intressant alternativ till de traditionella substratmaterialen. Papprets ytegenskaper kan modifieras med olika ytbehandlingsmetoder. Dessutom kan tryckning av funktionella material väl tillämpas på papper.

Målet med detta arbete var att utveckla en pappersbaserad studieplattform för biokemiska och biologiska analyser genom att modifiera ytegenskaper av bestrykt papper. Olika latexytor tillverkades genom att variera blandningsförhållanden av två latexkomponenter och genom att behandla latexytorna med infrarödstrålning. Ytegenskaperna och deras inverkan på proteinadsorption studerades. En latexyta med två höjdnivåer formades av hydrofob polystyren (PS) och hydrofil akrylonitrilbutadienstyrenkopolymer (ABS) med infrarödbehandling. PS-latex fanns adsorbera mera protein än ABS. Adsorption av avidin på ABS upptäcktes möjliggjöra högre specifika bindningsaktivitet jämfört med adsorption på PS-ytan.

Dessutom studerades cellernas tryckbarhet och cellväxt på de bestrykna papperssubstraten. ARPE-19 -, HepG2 - och Staphylococcus aureus -celler användes i cellstudierna. Latexbestrykningen fungerade som ett utmärkt substrat för celler. Avidin förminskade adhesion av bakterier till tvåkomponentlatex.

Publications

1 Enhanced protein adsorption and patterning on nanostructured latex-coated paper

Helka Juvonen, Anni Määttänen, Petri Ihalainen, Tapani Viitala, Jawad Sarfraz, Jouko Peltonen, *Colloids and Surfaces B: Biointerfaces, 118*, **2014**, 261–269.

2 Biocompatibility of printed paper-based arrays for 2-D cell cultures

Helka Juvonen, Anni Määttänen, Patrick Laurén, Petri Ihalainen, Arto Urtti, Marjo Yliperttula, Jouko Peltonen, *Acta Biomaterialia, 9,* **2013,** 6704–6710.

3 Protein and bacterial interactions with nanostructured polymer coatings

Helka Juvonen, Terhi Oja, Anni Määttänen, Jawad Sarfraz, Emil Rosqvist, Tiina Riihimäki, Martti Toivakka, Markku Kulomaa, Pia Vuorela, Adyary Fallarero, Jouko Peltonen, Petri Ihalainen, *Colloids and Surfaces B: Biointerfaces, 136,* **2015,** 527-535.

Supporting publications

S1 Film formation and surface properties of enzymatically crosslinked casein films

Helka Juvonen, Maria Smolander, Harry Boer, Jaakko Pere, Johanna Buchert, Jouko Peltonen, *Journal of Applied Polymer Science*, *119*, **2011**, 2205–2213.

S2 Fabrication of printed drug-delivery systems

Natalja Genina, Ruzica Kolakovic, Mirja Palo, Daniela Fors, Helka Juvonen, Petri Ihalainen, Jouko Peltonen, Niklas Sandler, *NIP29 29th International Conference on Digital Printing Technologies*, Seattle, Washington, **2013**.

S3 **Bioactive glass combined with bisphosphonates provides protection against biofilms formed by the periodontal pathogen *Aggregatibacter actinomycetemcomitans***

Adyary Fallarero, Anna Hiltunen, Malena Skogman, Kirsi Rosenqvist, Helka Juvonen, Petri Ihalainen, Jouko Peltonen, Anne Juppo, *International Journal of Pharmaceutics*, *501*, **2016, 211 - 220**.

Contribution of the author

The experimental work, analysis of the results and writing the first draft of the publications were carried out by the author with the following exceptions:

The flexographic and ink-jet printing experiments and the contact angle measurements were carried out by Anni Määttänen. The XPS measurements were conducted by Jawad Sarfraz. Patrick Laurén was responsible for the ARPE-19 and HepG2 cell cultures. The static biofilm method experiments were carried out by Terhi Oja. In Paper 1, the quartz crystal microbalance measurements were conducted by Tapani Viitala.

1. INTRODUCTION

Proteins are the most versatile macromolecules in the living systems. They are polypeptides that are composed of about twenty different amino acids in a sequence (primary structure) that forms repetitive 3D structures (secondary structure) like alpha helix, beta sheet and random coil structures. The final 3D structure of one protein unit is called the tertiary structure, and it plays a significant role in the protein functionality. Some proteins, e.g. (strept)avidin and C-reactive protein, are multiunit proteins consisting of non-covalently linked protein subunits [Zocchi 2003, Taylor 2007]. The quaternary structure of the protein refers to the arrangement of several protein units.

Proteins can be used as coatings on a substrate in order to take advantage of their biological functions like specific binding ability. When a protein molecule is brought in contact with the surface, the protein-surface interactions cause orientational and structural rearrangements which affect the function of the protein [Wang 2012]. The physicochemical surface properties of the substrate have an impact on the protein adsorption and its activity. These surface properties include topography, surface chemistry, charge and surface energy [van Oss 2003 a, Vogler 2012]. The important properties of the proteins affecting their adsorption behavior are the conformational stability, charge, hydrophobicity and the specific interacting residues [Wang 2012]. The complexity of the protein adsorption phenomenon arises from the interplay between the surface, the protein, and the adsorption conditions, such as temperature and pH.

The retained activity of adsorbed proteins is important in applications based on the biochemical immobilization, for example in (strept)avidin-biotin technology. (Strept)avidin has a stable structure and highly specific recognition sites for biotin and has enabled the use of avidin-biotin linkage in numerous bioanalytical applications, for example in biosensing and diagnostics, already for decades [Wilchek 1988]. Adsorbed proteins have been studied also for their ability to enhance or reduce cellular adhesion. Fibronectin, for example, is known for its specific interactions with

cells, whereas serum albumin is often observed to repel the cells [Plow 2000, Curtis 1984, Keogh 1994].

Cell adhesion is controlled by specific protein receptors that respond to the features of the extracellular matrix, such as availability and spatial distribution of adhesive ligands and surface topography [Liu 2009]. Understanding the cell-substrate interactions is important in e.g. the development of platforms for the cytotoxicity assays and biofilm studies. Antimicrobial paper has also been developed [Martins 2013]. Bacteria are responsible for severe threats to human health by colonizing a variety of surfaces, for example medical devices [Høiby 2014]. Adhesion of bacterial cells to a surface is the first step in the formation of biofilms that are well-organized communities of cells surrounded by a protective layer of self-produced extracellular polymeric substance. Controlling the initial step of the biofilm formation would be an effective strategy for the inhibition of biofilms formed by common bacteria, e.g. *Staphylococcus aureus* that forms highly tolerant biofilms [Donlan 2002]. *S. aureus* is frequently the cause of acute systemic infections, otitis media and persistent chronic pathologies, and it is the most common pathogen causing nosocomial diseases.

Cell and biofilm studies are conventionally performed on rigid substrates, such as glass and polystyrene. Scaffolds with certain topographical features for cell studies are often prepared with time consuming microfabrication methods such as hot embossing and lithography. Paper is an interesting alternative to conventional materials for cell studies [Ng 2016]. Paper is a widely used porous and flexible substrate and its chemical and physical surface properties can be modified by various surface treatments, such as conventional paper coatings, hydrogels or cell adhesive proteins [Kim 2015, Pelton 2009]. Proteins can be attached to the paper surface through physical immobilization, covalent coupling or biochemical immobilization. Paper is also well suited for printing of functional materials, e.g. drug substances, and can be used in the fields of printed diagnostics, immunoassays, and drug and toxicity research [Määttänen 2011, Parolo 2013, Pelton 2009, Sarfraz 2012]. The porosity of paper and the possibility to stack the paper sheets enables creating 3D cell cultures that have been used for

e.g. disease model studies and cryo-preservation of cells [Derda 2011, Ng 2016].

Using paper as a substrate and printing methods to introduce materials to the surface of the substrate would enable the development of cost-effective and high-throughput methods for producing platforms for cell studies and biofabrication. The biofabrication technology is widely used in biomedical applications such as tissue engineering [Mironov 2009]. As an example, a 2D scaffold-based manufacturing method has been used in order to create artificial skin and trachea [Chang 2011]. Broader reviews on the use of paper-based platforms in the fields of biomedical applications and diagnostics are given by Pelton, Parolo and Ng et al. [Ng 2016, Parolo 2013, Pelton 2009]

2. OBJECTIVES

In this work, protein adsorption and cell adhesion to coated paper substrates was studied. The aim of the study was to develop a paper-based test platform for biochemical and biological assays by modifying the surface properties of the coated paper, including topography and surface chemistry. Another objective was to correlate these surface properties to the adsorption behavior of proteins and cells.

In Paper 1, the aim was to investigate how the short-wavelength infra red (IR) treatment affected the surface properties of two-component latex coatings and adsorption of three model proteins. The ARPE-19 cell growth on four paper substrates with different surface characteristics was the objective of the research in Paper 2. The first aim of the study in Paper 3 was to modify the surface properties of the IR treated latex coatings by varied latex blend composition. The second objective of this study was to investigate the effect of the different latex surfaces on adsorption and activity of avidin. Thirdly, the research objective was to investigate adhesion of *S. aureus* to the latex surfaces with and without preadsorbed avidin. Additionally, printability of ARPE-19 and HepG2 cells by a screen-printing method was demonstrated (unpublished data).

3. SURFACE PROPERTIES

3.1. Surface topography

Surface features of many size scales affect the functionality of the surfaces [Czichos 2006]. The methods for characterizing the surface topography can be chosen according to the lengthscale of interest. The main methods to measure the surface topography are optical techniques and profilometers. Scanning probe microscopy includes both noncontact and contact methods. Atomic force microscopy (AFM) belongs to the family of scanning probe microscopy. The high lateral and vertical resolution (nano- to microscale) and the possibility to use low imaging forces make AFM well suited for protein and cell immobilization studies.

The surface topography can be described by means of 3-D areal roughness parameters [Blunt 2003, Blateyron 2013]. The areal roughness parameters are determined by using the data over the measured area. The areal roughness parameters, consisting of the surface parameters (S-parameters) and the volume parameters (V-parameters), are used to classify the surface topography by average and extreme properties and their deviations, spacing information and generic functional properties. The S-parameters describe the height and spatial properties and the V-parameters give information based on the material ratio curve (Figure 1). Four roughness parameters used in this work are described in the following. In addition, bearing area ratio was used in order to quantify the ratio between the top area and the total area of the surface that was estimated from the height histograms (Paper 2).

S_q is an amplitude parameter and is defined as the root mean square (RMS) value of the surface departures (z(x,y)) within the sampling area (A) [Blateyron 2013]. RMS roughness is very commonly used to describe the surface topography.

$$S_q = \sqrt{\frac{1}{A}\iint_A z(x,y)dxdy} \qquad (1)$$

S_{dr}, the surface area ratio, is a roughness parameter that describes the roughness-induced increment of the surface area relative to

the projected flat surface area [Blateyron 2013]. For a perfectly smooth surface, S_{dr} = 0. The S_{dr} parameter can be of use in wetting and adhesion studies, and the increment of the surface area contributes e.g. to the area available for adsorbate and thus to the loading capacity of the surface [Peltonen 2004, Löberg 2010].

The autocorrelation length S_{al} (also called S_{cl}) is a spatial parameter that is defined as the horizontal distance of the autocorrelation function (ACF(tx,ty)) that has the fastest decay to a specified value [Blateyron 2013]. This parameter is used to describe the spatial frequency of the surface features that can be of importance in e.g. cell adhesion.

$$S_{al} = min\sqrt{tx^2 + ty^2} \qquad (2)$$

The height distribution can be presented as a histogram that quantifies the number of points on the surface placed at a given height. The material ratio curve, also known as the Abbott-Firestone curve or the bearing ratio curve, is a cumulative curve of the height distribution that collects the information from the highest point (material ratio (mr) = 0 %) to the lowest point (mr = 100 %) of the surface (Figure 1) [Blateyron 2013]. The void volume parameter, V_v(mr), attributes to the void volume that is calculated for a defined mr, represented by the material ratio curve. Void volume can be used in order to evaluate the surface topography of materials to be used in contact with other materials [Blateyron 2013].

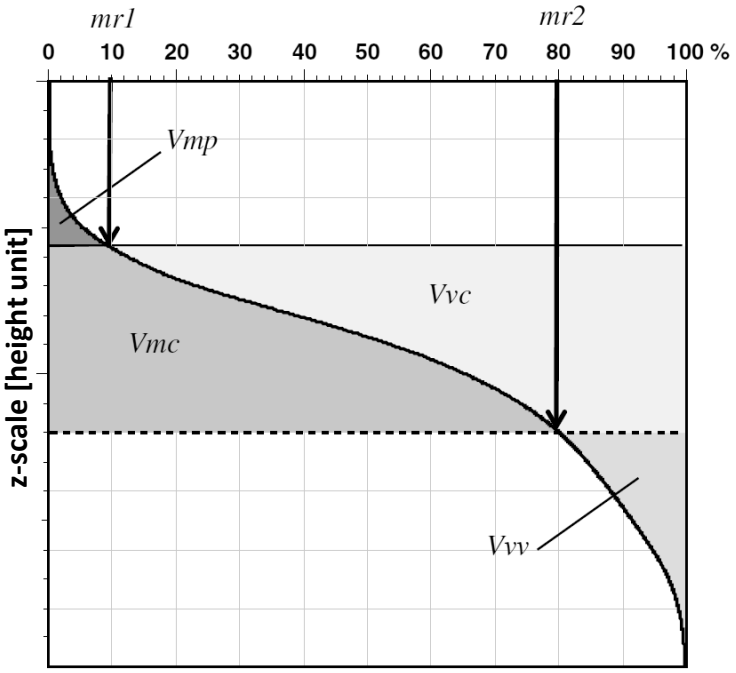

Figure 1. A material ratio curve. V_{mp} is the peak material volume, V_{mc} is the core material volume, V_{vc} is the core void volume, V_{vv} is the Dales void volume and mr denotes the material ratio [Blateyron 2013].

3.2. Wetting and surface energy

Wettability of a surface plays an important role in the interactions of cells and proteins with the surface. Hydrophobicity (water contact angle $\theta_W \geq 90°$), hydrophilicity ($\theta_W < 90°$) and the surface energy of the substrate have often been attributed to the adsorption of biological substances [Albers 2012, Vogler 2012]. Wettability and surface energy can be determined by the commonly applied sessile drop method.

A droplet of a liquid introduced on a solid surface in gas or vapor atmosphere can spread over and completely wet the surface, or it can form a droplet on the surface. At equilibrium with the surface, the droplet can be described by the contact angle, θ, which is the angle between the tangent to the liquid-vapor interface and the tangent to the solid-liquid interface at the contact line between

the three phases (Figure 2). The contact angle can be used to determine the surface energy of a solid surface.

Heterogeneities on the surface cause a discrepancy in the macroscopically detected contact angle (apparent contact angle) and the actual contact angle (Figure 2). For an ideally flat surface, the apparent contact angle equals the actual contact angle, and is called the Young contact angle, θ_Y. The Young contact angle and the interfacial tensions are correlated in the Young equation [Young 1805] as

$$\gamma_{SV} = \gamma_{LV} cos\theta_Y + \gamma_{SL} \quad (3)$$

where γ_{SV}, γ_{LV} and γ_{SL} are the interfacial surface tensions for solid-vapor, liquid-vapor and solid-liquid interfaces, respectively (Figure 2).

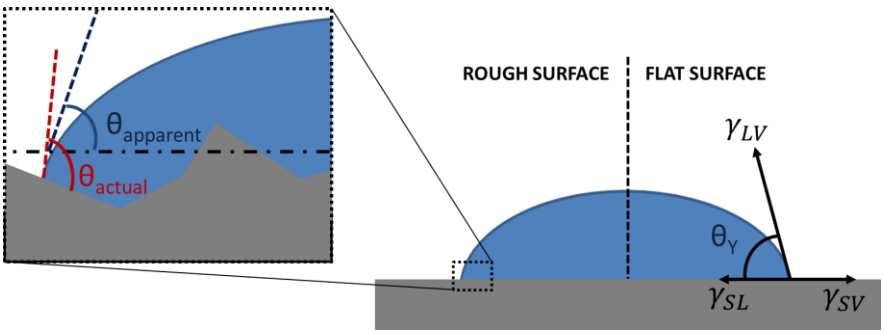

Figure 2. Actual and apparent contact angles and the interfacial tension components between a solid surface and a liquid in vapor atmosphere. Modified from [Marmur 2009].

The Young contact angle for a rough surface can be determined by the Wenzel equation [Wenzel 1936]

$$\cos\theta_A = r\ cos\theta_Y \quad (4)$$

where θ_A is apparent contact angle and *r* is a roughness factor, defined by Wenzel as the actual surface divided by the geometric surface.

The roughness factor r can also be defined with the help of the roughness parameter S_{dr} as described by Peltonen et al. [Peltonen 2004].

$r = 1 + S_{dr}/100.$ (5)

The solid-liquid interfacial energy cannot be measured directly and can be eliminated by combining the Girifalco-Good equation [Girifalco 1956]

$$\gamma_{SL} = \gamma_{SV} + \gamma_{LV} - 2\phi\sqrt{\gamma_{SV}\gamma_{LV}} \quad (6)$$

where ϕ is the interaction parameter, with the Young equation (3), resulting in

$$\gamma_{LV}(1 + cos\theta_Y) = 2\phi\sqrt{\gamma_{SV}\gamma_{LV}} \quad (7)$$

The interaction parameter ϕ is related to the dispersive and polar components of the surface energy by the Owens and Wendt theory, yielding

$$\gamma_{LV}(1 + cos\theta_Y) = 2\sqrt{\gamma_{SV}^d\gamma_{LV}^d} + 2\sqrt{\gamma_{SV}^p\gamma_{LV}^p} \quad (8)$$

where γ^d is the dispersive and γ^p the polar component [Owens 1969].

$$\gamma = \gamma^d + \gamma^p \quad (9)$$

In order to solve the surface energy components, two probe liquids with known surface tension components are needed in the Owens-Wendt method.

The surface energy can be divided also into Lifshitz-van der Waals (γ^{LW}) and acid-base (γ^{AB}) components, as derived in a method by van Oss, Chaudhury and Good [van Oss 1988].

$$\gamma = \gamma^{LW} + \gamma^{AB} \quad (10)$$

where

$$\gamma^{AB} = 2\sqrt{\gamma^+\gamma^-} \quad (11)$$

and γ^+ and γ^- are the Lewis acid (electron acceptor) and Lewis base (electron donor) components, respectively. The van Oss-Chaudhury-Good method gives

$$\gamma_{LV}(1 + cos\theta_Y) = 2\sqrt{\gamma_{SV}^{LW}\gamma_{LV}^{LW}} + 2\sqrt{\gamma_{SV}^+\gamma_{LV}^-} + 2\sqrt{\gamma_{SV}^-\gamma_{LV}^+}$$

Three probe liquids are required for solving the surface energy components by the van Oss-Chaudhury-Good method.

The challenges of wetting studies and surface energy determination include several aspects that one needs to be aware of [Marmur 2009]. The models are developed for an ideal surface that is defined as horizontally flat, rigid, chemically homogeneous, nonporous, insoluble and nonreactive. Generally, real surfaces do not fulfil this definition. For example, the effect of roughness on the contact angles can be estimated with the help of other surface characterization methods, such as AFM, and by using equation (5). On heterogeneous surfaces, the liquid droplet may adopt one of the energetically metastable states and the measured contact angle may differ from the contact angle of the most stable equilibrium. Moreover, the liquid droplet deposited on the surface is assumed to be symmetrical, which is not necessarily the case on heterogeneous surfaces. In order to ensure the symmetry, a sufficiently large droplet size relative to the scale of surface heterogeneity is required. In addition, the chosen probe liquids can have a tremendous effect on the obtained surface energy values. Finally, the different calculation methods may result in different surface energy values [Zenkiewicz 2007].

4. IMMOBILIZATION OF PROTEINS AND CELLS

Adsorption of material is affected by the interplay of the properties of the surface and the adsorbate and, in addition, the adsorption conditions like temperature. The chemical and biochemical complexity of the materials from biological origin makes it challenging to predict their adsorption behavior. Furthermore, the surface of the living organisms tends to change continuously with a response to the surrounding environment. However, the adsorption processes are based on the general physico-chemical interactions between the adsorbate and the surface.

Most commonly, rigid microwell plates made of polystyrene or other polymer materials are used for biochemical assays and cell-based assays. Further functionalization or coating of microwell plates is needed for the optimal immobilization. For example,

sulfhydryl groups and polylysine are used in order to enable covalent and ionic interactions, respectively. Besides chemistry, surface roughness affects the immobilization. Paper appears to be an interesting substrate for various bio-assays because the surface chemistry and topography of paper can be quite conveniently modified by different coating and printing methods. Additionally, it is possible to print array structures on paper, which enables its use as a substrate for various test platforms.

Adsorption may occur through physisorption or chemisorption. In addition, immobilization of biomolecules may occur through non-covalent specific receptor-ligand interactions. In this work, proteins are immobilized to the surfaces by physisorption or specific receptor-ligand interactions. The nature of immobilization in the cases of proteins and cells is discussed in this chapter.

4.1. Non-covalent interactions

Non-covalent interactions include van der Waals forces, hydrophobic and electrostatic interactions and hydrogen bonding (Figure 3) [Somorjai 2010]. In physisorption, the material is adsorbed non-specifically and non-covalently to the surface and adsorption takes place reversibly.

Van der Waals interactions are interactions between dipoles or induced dipoles and they are always present between materials. Van der Waals forces include long-range dispersion (London), Keesom and Debye forces.

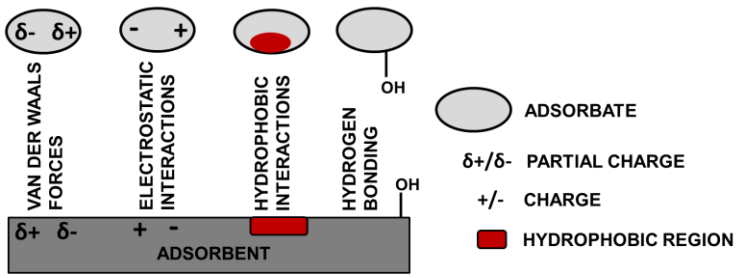

Figure 3. Non-covalent interactions.

Hydrogen bonding or Lewis acid-base interactions between two electronegative atoms sharing a proton is a combination of electrostatic and charge-transfer interactions. In contact with aqueous solution, the surface first hydrates with a layer of water molecules [Vogler 2012, Somorjai 2010]. The adsorbate needs to replace surface-bound water in order to allow the protein-surface interactions and adsorption. This energy barrier is related to the number of water molecules that are needed to be replaced and the hydrogen bonding strength between water molecules and hydrophilic groups of the surface and the protein. Hydrophilicity of the surface indicates the energy demanded for an adsorbate to compete with the water molecules in a way that replacing water by adsorbate is more favourable on hydrophobic than on hydrophilic surfaces. Consequently, the adsorbed material may often be replaced more easily on hydrophilic surfaces compared to hydrophobic surfaces. On the hydrophobic surfaces, the adsorption can be practically irreversible.

The thermodynamic approach has been used to explain an observation where, in many cases, the increased hydrophobicity of the surface enhances the attachment of proteins and cells [Katsikogianni 2004]. The water molecules are ordered close to hydrophobic surfaces and when they are released to the bulk solution, the entropy of the system increases. This results in free energy decrease causing enhanced adhesion on hydrophobic surfaces [Tsapikouni 2008]. Moreover, the hydrated cations that are bound to negatively charged surfaces contribute to the thermodynamics of the material-surface interaction by causing a repulsive hydration force upon adsorption [Valle Delgado 2011].

Hydrophobic interactions cause the aggregation of hydrophobic solutes in a hydrophilic solvent by minimizing the hydrophobic-hydrophilic interfacial area in order to decrease the total free energy. In general, the hydrophobicity of the surface is shown to increase the adsorption of proteins and cells, which is attributed to the hydrophobic interactions between the surface and the hydrophobic regions of the adsorbate.

Long-range electrostatic interactions may cause attraction or repulsion between a charged surface and a protein. For two

surfaces with similar charges the interaction is repulsive, whereas for opposite charges the interaction is attractive [Myers 1999]. In electrolyte solution, an electrical double layer is formed on the charged species. The counter-ions are attracted to the charged surface from the solution forming an essentially immobile layer (Stern layer). The concentrated (compared to the bulk solution) mobile layer of ions close to the Stern layer is called a diffuse double layer. The Stern layer and the diffuse double layer are divided by a shear plane. From the practical point of view, the ionic strength of the solution is an important factor that may determine the final strength of the electrostatic interactions. The increasing electrolyte concentration causes a faster decay of the surface potential over the distance from the surface. The charge interaction distances between the protein and the surface can thus be decreased in high ionic strength solutions.

Adsorption of proteins and cells can be prevented using biorepellent or bioinert coatings that repel the protein-induced adhesion of organisms [Banerjee 2011, Wei2014]. The molecular-level characteristics of protein-resistant surfaces include the presence of polar functional groups, the presence of hydrogen bond acceptor groups, the absence of hydrogen bond donor groups, and the absence of net charge. This type of polymer coatings should provide an additional hydration layer that prevents protein adhesion to the surface. In addition, the surface energy and the mobility of the polymer chains may play a significant role in preventing adsorption of proteins and cellular adhesion. For example, PDMS that is known as an antifouling material has a flexible backbone and very low surface energy [Liu 2009, Ji 2000].

4.2. Protein adsorption

Protein adsorption to the surface can occur by chemisorption via ionic or covalent bonding or non-covalently by physisorption and specific receptor-ligand interactions (Figure 4) [Zhu 2003, Pelton 2009]. Physisorption arises from the weak van der Waals interactions and the typical enthalpy for a small molecule (-20 kJ/mol) is lower compared to that of chemisorption (-200 kJ/mol)

[Atkins 2010]. However, physisorption plays an important role in the adsorption processes of macromolecules.

Specific receptor-ligand interactions are often involved in adsorption of the biological constituents (molecular recognition) and arise from e.g. hydrogen bonds, salt bridges, van der Waals interactions and the shape and complementarity of the interface [Kastritis 2015]. The strength of these interactions, i.e. the binding affinity, is physico-chemically announced as the dissociation constant (K_d) that equals the concentration of the free protein that occupies half of the overall sites of the second protein at equilibrium. The biochemical immobilization through specific interactions may lead to a uniform orientation of an adsorbate and is applied in affinity-based technology, such as in (strept)avidin-biotin technology. As an example, functional chemical or biochemical substances can be biotinylated and, subsequently, immobilized to surfaces that are pre-coated with avidin.

The protein adsorption process consists of the following steps: transport to the solid surface, attachment, structural and/or orientational changes and possible detachment and transport from the solid surface. The immobilization method and the surface-induced alteration of protein structure may affect the orientation, packing density and activity of the adsorbed protein.

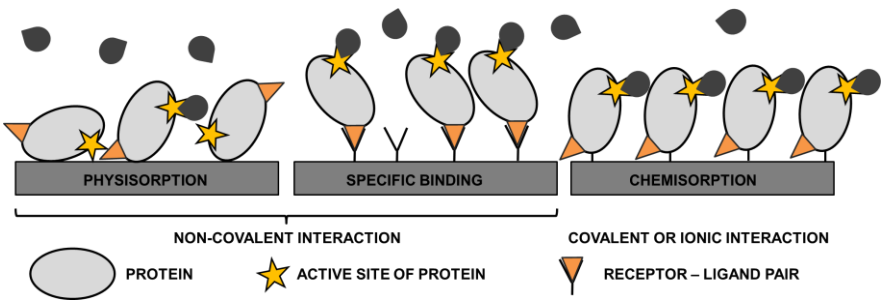

Figure 4. Protein adsorption by physisorption, specific binding and chemisorption. Modified from [Zhu 2003].

Chemisorption may involve irreversible chemical binding and provides stable adsorption and high surface loading, compared to non-covalent adsorption [Williams 1994]. The primary amine,

sulfhydryl, carboxylate and phenolate groups on protein are commonly used for immobilization via covalent binding [Aydin 2012].

The orientation, packing and surface-induced deformation of the adsorbed proteins can influence the accessibility of the binding sites of the proteins. As a result, the binding behavior of the ligand may be changed upon adsorption (Figure 5). For example, small spacing between the adsorbed proteins, i.e. tight packing may make the specific binding sites unavailable for the ligand through steric hindrance. The steric effects can be more easily controlled by specific binding or chemisorption than by physisorption that often results in random orientation. On the other hand, chemisorption may cause more protein denaturation than non-covalent adsorption [Williams 1994].

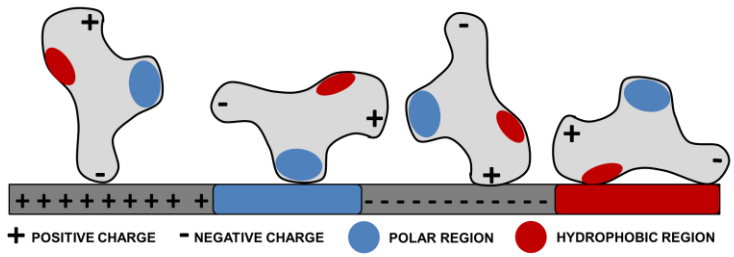

Figure 5. Orientation of proteins influenced by the surface properties of the substrate and the protein. Modified from [Dee 2002].

Proteins consist of positively and negatively charged peptides that give a net electric charge that is dependent on the pH and the ionic strength of the solution. At certain pH (isoelectric point, IEP), the net charge of the protein is zero. The IEP can thus be used to predict the electrostatic interactions between the protein and the adsorbent. The local charged regions of the protein may, however, dominate and the proteins may adsorb electrostatically despite the apparently unfavorable net charge [Goy-Lopez 2012, Jachimska 2012].

Proteins are structurally complex macromolecules that are prone to denaturation, which can lead in changes of the specific biochemical activity [Somorjai 2010]. Hydrogen and disulfide bonds

retain the secondary structure of polypeptide chains, while the tertiary structure is a result of the electrostatic and hydrophobic interactions [Tsapikouni 2008]. As stated previously (section 4.1.), proteins tend to adsorb more preferably to hydrophobic surfaces than to hydrophilic surfaces. Some proteins are structurally more unstable than others and can easily undergo conformational rearrangements (sometimes called “soft” proteins). This kind of structural flexibility may enable protein adsorption also to hydrophilic or even to electrostatically repellent surfaces [Norde 1992].

In fact, the complexity of protein structure exists in many levels and the “soft” and “hard” regions coexist in proteins. The majority of the proteins consist of one or more domains that have a distinct structure, function or evolutionary history [Ekman 2005]. A domain can be defined as an independently folding unit. Repeats of same type of domains are common in multi-domain proteins. Both ordered regions, such as α-helices, β-sheets and coils, and disordered regions exist within and outside of the domains. The location of the different structural regions of proteins together with the surface properties of the substrate may thus affect the protein orientation and conformation on the surface.

Multiple adsorption sites may result in the structural deformation of the adsorbed protein. Surface-induced denaturation of a protein may inactivate the binding sites or, on the other hand, make the binding sites, initially inaccessible, available for specific binding (Figure 6).

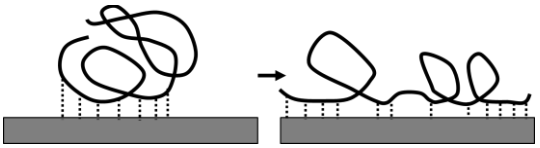

Figure 6. Surface-induced denaturation of the protein. Modified from [Dee 2012].

Proteins are commonly known to adhere to hydrophobic surfaces due to the hydrophobic interactions between the protein core and the surface [Kamiya 2014, Albers 2012]. The surface-induced structural changes are often due to the hydrophobic surface-protein interactions. A protein folds in its native state with the

hydrophobic regions buried inside its core and the hydrophilic segments mostly covering the surface where they form hydrogen bonds with water molecules. The hydrophilic residues are able to form hydrogen bonds with a hydrophilic substrate, and protein adsorption via hydrogen bonding mostly occurs at polar surfaces. Protein adsorption can thus be enhanced by increasing the hydrogen bond donors on a substrate [Chapman 2000]. Moreover, the electrostatic interactions may also induce denaturation of the protein. Near the surface, the electrostatic potential or the surface energy may affect the intramolecular bonds, followed by binding to the substrate and unfolding of the protein.

Topography of the surface has been shown to affect the conformation and the amount of adsorbed proteins [Lindman 2007, Rockwell 2012]. The structure of the proteins can be affected by the radius of curvature of the surface that may either stabilize or denature the proteins. In addition to the conformational effects, the roughness-induced increase in the surface area results in a larger protein loading capability of the surface.

The protein-protein interactions have a stabilizing effect on the protein structure (Figure 7) [Vogler 2012, Seigel 1997, Kamiya 2014, Albers 2012]. These interactions are enhanced by high protein concentrations and may also be increased by the conformational changes due to the hydrophobic interactions on a hydrophobic surface, which can result in formation of protein agglomerates. Proteins that are adsorbed from low concentrations obtain less stabilizing protein-protein interactions and denature more easily upon adsorption.

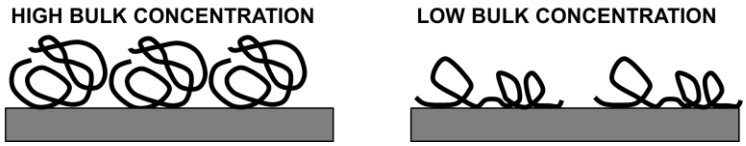

Figure 7. Effect of the protein-protein interactions on protein stability. Modified from [Dee 2002].

4.2.1. (Strept)avidin

Avidins are proteins that are able to bind specifically biotin, also known as vitamin H or vitamin B_7, with a high affinity [Green 1990, Green 1975]. Chicken avidin is a basic and tetrameric glycoprotein that is found in chicken egg white [Zocchi 2003]. Each of the four subunits of chicken avidin is singly glycosylated. The molecular weight of chicken avidin is 66 kDa, size 4 × 5.5 × 6 nm, and the isoelectric point (IEP) is 10.0 ± 0.5 [Vikholm-Lundin 2012]. Streptavidin from *Streptomyces avidinii*, a protein without carbohydrate chains, is one of the bacterial analogs of avidin. Streptavidin has a molecular weight of 60 kDa and slightly acidic or near-neutral IEP [Diamandis 1991, van Oss 2003 b]. The strength of the (strept)avidin-biotin interaction results from several hydrogen bonds, hydrophobic contacts and complementary shape of these biomolecules [Livnah 1993]. (Strept)avidin can be considered to be a structurally relatively stable protein and it is not likely to undergo any significant rearrangement upon adsorption. The stability of (strept)avidin, together with its recognition sites for biotin, makes it an attractive biomolecule for many applications. The biotinylation of the chemical and biological substances and the adsorption of (strept)avidin to surfaces enable applications that are based on the strong interaction between (strept)avidin and biotin [Wilchek 1988]. This strong (strept)avidin-biotin linkage has been used in numerous bioanalytical applications, such as immunodiagnostics and biosensing [Wilchek 1988]. Use of streptavidin is often preferred in comparison to chicken avidin due to its lower non-specific binding characteristics.

4.2.2. Albumin

Serum albumin (65 kDa) is a water soluble protein and the most abundant protein in mammalian blood serum [Scott 1988]. The isoelectric point of serum albumin is about 5.0 and it is negatively charged in pH 7 [Tran 2012]. Albumin is approximately an equilateral triangle with sides of about 8.0 nm and a thickness of about 3.0 nm [Carter 1989]. Serum albumin is a “soft” protein, i.e., it is able to undergo structural rearrangements easily upon adsorption. Albumin contains hydrophilic and hydrophobic, as well

as charged and uncharged regions, which together with the flexible structure enables adsorption to many types of surfaces [D´Sa 2010]. Serum albumin is known to be a biomaterial repellent protein and a pre-adsorbed albumin layer reduces the adsorption of other proteins and cells [Curtis 1984, Keogh 1994].

4.2.3. Fibronectin

Fibronectin (~500 kDa) is a glycoprotein existing as a covalently linked dimer of two nearly identical subunits of about 250 kDa [Pankov 2002]. The IEP of fibronectin is about 5.0. Fibronectin is found as a soluble form in plasma and as an insoluble, fibrillar form in extracellular matrix. In plasma, fibronectin has been reported to appear in globular, disc-like and filamentous forms [Williams 1982]. In physiological conditions, fibronectin has been shown to adopt a folded but at the same time an elongated form [Sjöberg 1989]. It is known as a cell adhesive protein that can serve as a ligand for several integrins, i.e. the receptors that link the extracellular matrix with the intracellular cytoskeleton [Plow 2000]. Fibronectin is a flexible protein and it is able to adopt various conformations upon adsorption [Österlund 1988, Belegrinou 2008]. The ability to bind integrins by fibronectin is often retained upon adsorption, although the extent of the biological functionality of adsorbed fibronectin is affected by the surface properties of the substrate [Ribeiro 2012, Kowalczynska 2007].

4.3. Cell adhesion

Cell growth, viability and proliferation on a surface are affected by the properties of both the cell and the surface (Figure 8) [Klee 2000, Feinberg 2008]. Different cell types respond in a characteristic fashion to, e.g., the surface topography, chemistry, wetting, and surface energetics [Klee 2000, Flemming 1999, Redey 2000, Kaelble 1977, Satriano 2003, Otsuka 2000]. Surface roughness may affect the cell adhesion in a positive or negative manner, depending on the cell type and the length scale of the roughness [Webb 2013]. Epithelial cells adhere more preferably to smooth than to rough surfaces, whereas increased roughness has been found to promote adhesion of certain bacterial cells

[Baharloo 2005, Müller 2007]. Surface chemistry and the distribution of the chemical groups over the surface play a role in optimal adhesion of cells. Surface chemistry also directly affects wetting properties and surface energy. The effect of wetting on cell adhesion is also dependent on the cell type. For example, endothelial cells have been reported to prefer adhesion to hydrophilic surfaces and, on the other hand, *S. aureus* bacteria adhere better to hydrophobic surfaces [Chibowski 2000, Redey 2000, Satriano 2003, Vogler 1998, Müller 2007, Tegoulia 2002]. Furthermore, adsorption of proteins from e.g. a cell medium may enhance or reduce cell adhesion [Satriano 2003]. Typically, cell adhesive proteins, such as fibronectin, are used to enhance cell attachment, whereas BSA is known as a cell-repellent protein [Plow 2000, Curtis 1984, Keogh 1994].

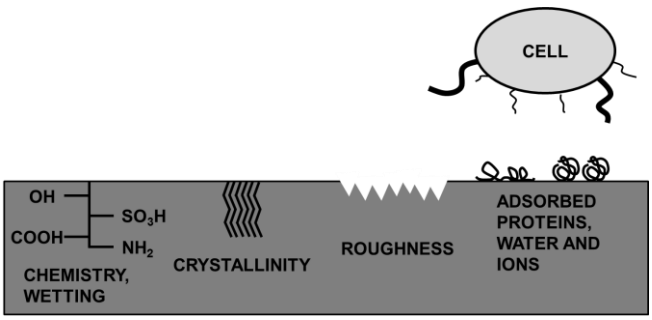

Figure 8. Factors influencing cell-surface interactions. Modified from [Klee 2000].

Cells are transported from liquid to a solid surface by long-range, non-specific physical interactions like gravity, van der Waals forces, acid-base interactions, electrostatic forces, and Brownian motion [Gottenbos 2002]. For example, positively charged poly-L-lysine (PLL) is often used for functionalization of surfaces in order to promote the cellular adhesion by an electrostatic attachment of biomolecules. PLL is a positively charged synthetic polypeptide of amino acid L-lysine [Morga 2015]. The amino groups of PLL can be easily protonated resulting in a positive charge over a broad pH range.

In a close cell-surface contact, the short-range physicochemical interactions such as hydrogen bonding and specific interactions become effective [Katsikogianni 2004]. The specific interactions

caused by the biochemical or chemical substances have an influence on the surface properties and thus cell adhesion. The cell wall consists of a variety of biomolecules that participate in the interactions with the surroundings. Natural cell membranes consist of a zwitterionic phospholipid bilayer that contains batches of carbohydrates and proteins [Wei 2014]. The receptor-ligand interactions play an important role when the cell is attaching to the preadsorbed biomolecules like proteins. The specific interactions with the preadsorbed overlayer may rule out the effect of the physicochemical properties of the underlaying surface.

4.3.1. ARPE-19 cells

The ARPE-19 cell line is derived from the retinal pigment epithelium (RPE), the outermost layer of the retina of a 19-year-old male donor [Dunn 1996]. The ARPE-19 cells form epithelial monolayers on solid supports and are thus well suited for the studies on planar substrates. The attachment of the ARPE-19 cells to solid surfaces is affected by the wettability and roughness of the surface. The smooth and hydrophilic surfaces have been found to support the adhesion of ARPE-19 cells [Oliver 2009].

4.3.2. HepG2 cells

HepG2 derived from the liver carcinoma of a Caucasian male is one of the most frequently used cell lines. The HepG2 cells are adherent with an epithelial cell morphology enabling their use in cell studies on surfaces. They grow as monolayers and in small aggregates [ATCC, HepG2.com]. Cell lines developed from hepatocellular hepatomas are commonly used in toxicity studies that could be an interesting application area for paper-based platforms.

4.3.3. *S. aureus* bacterial cells

S. aureus is a spherical prokaryotic cell that easily forms bacterial clusters and highly tolerant biofilms. *S. aureus* is a common pathogen that is able to colonize a variety of surfaces [Lister 2014, Kiedrowski 2011]. It causes acute systemic infections as well as

chronic pathologies, and it is able to persist on different surfaces. Understanding and controlling the biofilm formation of *S. aureus* would be beneficial in e.g. medical implant applications.

A relatively rigid cell wall with a net negative surface charge at neutral pH surrounds the single *S. aureus* bacteria. The presence of positively charged D-alanine esters and negatively charged phosphate groups results in a bipolar nature of a bacterial cell wall which leads to the ability to interact with various surfaces. Adhesion of *S. aureus* is enhanced by the increased roughness and the dominance of hydrophobic interactions.

5. MATERIALS AND METHODS

5.1. Substrates

5.1.1. Latex coatings and their substrates

Two different aqueous latex dispersions, polystyrene (PS) and carboxylated acrylonitrile butadiene styrene copolymer (ABS), and their blends were used for the latex coatings. Both of the latex components were emulsion polymerized. The ABS (film-forming) component was a copolymer with glass transition temperature T_g = 8–10◦C (DL920, DOW Europe GmbH, d = 140 nm). The PS (nonfilm-forming) component was polystyrene with T_g > 90◦C (DPP3710, DOW Europe GmbH, d = 140 nm in Papers 1 and 2; HPY83, Styron Europe GmbH, d = 130 nm in Paper 3). The two-component PS:ABS latex blends were prepared by mixing the PS and ABS components so that the weight ratios (wt%) in the blend were 20:80, 30:70, 40:60, 50:50 and 60:40.

A base paper (Veitsiluoto, Finland) with a ground calcium carbonate (Hydrocarb 90, Omya AG) precoating was used as a paper substrate for latex coatings in Paper 2. In Papers 1 and 3, a multi-layer curtain coated paper including a coated barrier layer was used as a paper substrate [Bollström 2012]. The latex blend was applied on the base paper substrate by a rod-coater (K Control Coater, RK Print-Coat Instruments Ltd., UK) or a roll-to-roll reverse gravure coater (RG, a custom-built roll-to-roll RG coater). The latex-

coated paper was dried immediately after coating by radiating it with a short-wavelength infrared (IR) lamp (IRT-010, 1 kW, IRT systems, Hedson Technologies AB, Sweden) for 4 seconds. The IR lamp was positioned at about 20 cm distance from the sample. This sample is referred to as “pristine”. The samples were also IR-treated for a longer period of time (60 s) with the same IR lamp. The peak temperature was around 180◦C at the surface. This sample is referred to as “IR-treated”. The single-component coatings containing only the ABS or the PS latex were fabricated through the same procedure as the two-component blend. The latex coatings were rinsed with water and ethanol prior to further analysis and treatments.

Gold-coated AT-cut quartz crystals with a nominal frequency of 5 MHz (Biolin Scientific AB, Q-sense, Sweden) were used for the QCM measurements. The crystals were cleaned by rinsing with ethanol and water, followed by drying with nitrogen gas (Papers 1 and 3). Latex, either pure ABS or a two-component blend, was spin-coated on the quartz crystal by dispensing a diluted latex dispersion (5:1 water:latex volume ratio) on top of the quartz crystal and by rotating the crystal at a speed of 1000 rpm for one minute. In Paper 1, this was followed by rotation at 9000 rpm for 10 seconds. Pristine latex coatings and IR-treated latex coatings with IR treatment for 25 seconds were prepared. The latex coatings were rinsed with water and ethanol prior to the QCM measurements.

5.1.2. Pigment coatings

Three different pigment top coatings were used as the substrates for the cell studies in Paper 2. Precipitated calcium carbonate (PCC) was used as a component in one of the coatings. The second top coating consisted of kaolin (Barrisurf HX, Imerys Ltd.) and a latex binder (Aquaseal 2077, Paramelt) [Bollström 2009]. The third coating consisted of a mixture of two different kaolin pigments (Barrisurf FX, Imerys Ltd. and Alphatex, Imerys Ltd.) and latex binder (Basonal®, BASF).

5.1.3. Paper-based test arrays

Patterned test arrays were printed by using PDMS due to its antifouling surface properties [Liu 2009, Ji 2000]. A three-component ink consisting of PDMS with vinyl groups (Dehesive® 920), a Wacker® catalyst OL and a crosslinker V24 with a weight ratio of 100:2.5:1 (Wacker Chemie, AG, Germany) was flexographically printed on the pigment-coated paper and IR-cured [Määttänen 2011]. The areas remaining unprinted by PDMS formed a matrix of circles with a diameter of 2 mm, 5 mm, or 7 mm (Figure 9). These unprinted, PDMS-free circles acted as test areas for cell culture.

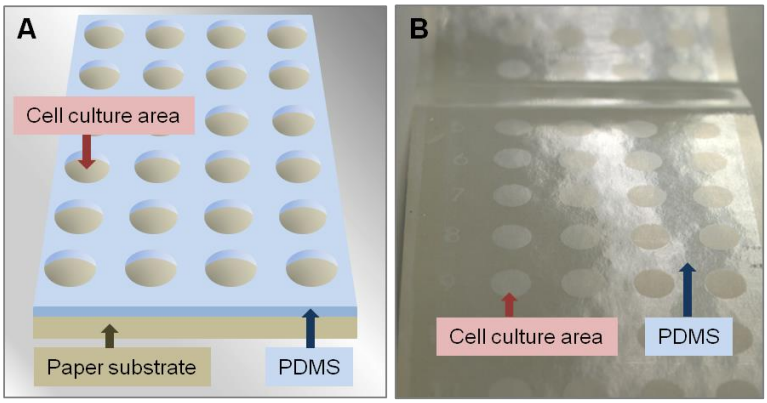

Figure 9. Printed test platforms for cell studies. A schematic image (a) and a photograph (b) of the array of circular test areas (diameter 5 mm) surrounded by printed PDMS. Paper 2.

5.1.4. Plasma- and poly-L-lysine treated polystyrene

For the screen-printing tests, the polystyrene microscopy slides were modified with poly-L-lysine (PLL) and plasma in order to ensure the wettability of the substrate by the bioink (unpublished data). Polystyrene microscope slides (PS slide) were coated with poly-L-lysine (Trevigen Cultrex, 70 – 150 kDa) by immersing the slides in a solution of 0.01 % PLL in phosphate buffered saline (PBS, Dulbecco's modified phosphate buffer without calcium and magnesium) for two minutes. The excess of PLL solution was drained off and the PS slides were dried in ambient conditions for 4

h, washed with water (ultrapure milliQ water) twice and dried with pressurized air. The PLL-coated PS slides were sterilized by air plasma treatment (Harrick Plasma Cleaner/Sterilizer PDC-326) for two minutes.

5.2. Protein immobilization

Protein adsorption to the latex-coated paper substrates was carried out in a custom-built liquid chamber (diameter 7 mm). Proteins were adsorbed from either a phosphate buffer (50 mM, pH 7, $HNa_2O_4P{\cdot}2H_2O$, Fluka and $H_2NaO_4P{\cdot}H_2O$, Sigma-Aldrich with 100 mM NaCl) or a HEPES-EDTA buffer (10 mM HEPES (Sigma), 150 mMNaCl (Fluka), 1 mM EDTA (Sigma), pH 7.4) (Table 1). The immobilization was carried out at 22 ± 2˚C. After adsorption, the samples were rinsed with purified water (MilliQ) and dried with nitrogen gas.

Table 1. Protein adsorption to the latex coated paper substrates.

Protein	Buffer	pH	c [µg/ml]	Vol. [µl]	Ads. time [min]
Avidin(*	Phosphate	7.0	0.35, 3.5, 10, 35, 100, 350	200	60
Strept-avidin(**	HEPES-EDTA	7.4	2	100	20
BSA(**	HEPES-EDTA	7.4	1000	100	20
FN(**	HEPES-EDTA	7.4	30	100	20

*) Paper 3
**) Paper 1

5.2.1. (Strept)avidin adsorption

Avidin solutions containing wild type avidin from chicken egg (Belovo S.A., Bastogne, Belgium) were used with concentrations of 0.35 µg/ml to 350 µg/ml (Paper 3). Streptavidin from *Streptomyces avidinii* was purchased from Sigma (Paper 1). The concentration of the streptavidin solution was 2 µg/ml for protein immobilization to

a paper coating, whereas concentrations of 2 µg/ml and 100 µg/ml were used for QCM measurements.

For the bacterial adhesion studies, 100 µl of avidin (350 µg/ml in 50 mM phosphate buffer) was pipetted on the test areas of the cell study platform. Similarly, avidin that had been incubated three times in boiling water for 10 min was applied to the test area in order to coat the surface of the test area with denatured avidin. After an adsorption period of 30 min, excess avidin was rinsed off with 100 µl of phosphate buffer, followed by three further 1 min washing periods with 100 µl of ultrapure water. The samples were left to air-dry in ambient conditions overnight.

5.2.2. Serum albumin adsorption

Bovine serum albumin (BSA, Sigma) was used at a concentration of 1 mg/ml for the adsorption studies (Paper 1). Non-specific and specific adsorption of human serum albumin (HSA, Sigma) and biotinylated BSA (biotin-BSA) to pre-adsorbed avidin was studied at the albumin concentration of 100 µg/ml (Paper 3). The calculated conjugation ratio of biotin-BSA was 1:1 n(biotin):n(BSA).

5.2.3. Fibronectin adsorption

Fibronectin from bovine plasma (Sigma) was adsorbed to the latex surfaces from a solution with a concentration of 30 µg/ml (Paper 1).

5.3. Cell experiments

5.3.1. ARPE-19 and HepG2

Human adult retinal pigment epithelia cells (ARPE-19 cells, ATCC CRL-2302) were cultured in DMEM-F12 (1:1) supplemented with 10% fetal bovine serum, 2mM L-glutamine, 100 U/ml penicillin and 100 µg/ml streptomycin. Human hepatocellular carcinoma cells (HepG2, ATCC HB-8065) were cultured in high glucose Dulbecco's modified Eagle's medium supplemented with 10% fetal bovine serum, 100 µg/ml streptomycin, 100 U/ml penicillin, 100 mM

sodium pyruvate and 2 mM L-glutamine. Cell lines were cultured at 37 °C in a humidified incubator equilibrated with 7% CO_2.

ARPE-19 cell growth was studied on four different types of coated paper substrates. The printability of ARPE-19 and HepG2 cells was examined with screen printing and the viability of the printed cells was followed for 72 hours. Plasma treated poly-L-lysine coated polystyrene slides and a two-component latex coated paper were used as substrates for printing.

ARPE-19 cells were seeded on 2-D cell arrays printed on different paper substrates at a cell density of 160 000 cells/cm^2 (Paper 2). Three replicates were made and incubated in above mentioned conditions for 24, 48 and 72 h.

The screen printing of suspensions of ARPE-19 and HepG2 cells in matrigel (1:4 in cell culture medium) was conducted by a TIC Screen Printer (SCF-260B, Technical Industrial Co.) immediately after the plasma treatment of PLL-coated PS slides (unpublished data). The used dilution proportion resulted in a screen-printable ink formulation. A polyurethane squeegee (Serilor® 3500×25×05 soft) and a screen of monofilament polyester (Sefar PET 1500 110/280-40) with a nominal thread diameter of 40 µm, a mesh opening of 47 µm and a theoretical ink volume of 17.3 cm^3/m^2 were used. A screen with a mesh opening of 77 µm was also tested. The screen with the smaller mesh opening was chosen due to the better print quality. The squeegee and the mesh were sterilized with 70 % ethanol prior to printing. Duplicates were prepared for each of the incubation time point (24 h and 72 h).

After the incubation, cells were fixed in 2% paraformaldehyde for 15 min at room temperature and washed with PBS for three times. Depending on the substrate, the cells were stained with Hoechst 33342 or 3,3'-dioctadecyloxacarbocyanine perchlorate (DiO). On transparent polystyrene substrates, the cell nuclei were stained with a Hoechst 33342 dye (1 µg/ml) and washed three times with PBS. Lipophilic DiO was chosen for staining the membranes on paper since a hydrophilic dye would have adhered to the paper substrate and caused a background signal. Additionally, the autofluorescence of the paper samples did not cause disturbing background at the fluorescence emission region of DiO (500 – 550

nm). DiO was dissolved in ethanol (35 µg/ml) and diluted in purified milliQ water to the working concentration of 5 µg/ml. Two-dimensional cell arrays were incubated in a DiO solution for 1 h at room temperature and washed three times with PBS. The stained cells were observed with a fluorescence microscope (Nikon Microphot EPI-FL3, Japan) with a magnification of 10 or 20.

The viability of the printed cells was studied with Alamar blue (10 % of the sample volume, 3.5 h of incubation). The fluorescence was monitored with an excitation wavelength of 540 nm and emission of 590 nm with a PerkinElmer Luminescence spectrometer (LS50B).

5.3.2. *S. aureus*

Bacterial adhesion experiments of *S. aureus* (ATCC 25923) to the latex substrates were conducted mainly by using the static biofilm method (Paper 3) [Oja 2014]. Filter-covered tryptic soy agar (TSA, Sigma-Aldrich) plates were inoculated by pipetting 1.5 ml of the *S. aureus* preculture diluted with TSB to a bacterial concentration of about 1×10^8 CFU/ml (colony forming units). The substrates for the bacterial studies were cleaned by dipping in sterile ultrapure water and air-dried in a laminar hood for 15 to 30 min. The substrates were then placed on the inoculated plates to allow the bacterial adhesion to the test area of the cell study platform and incubated for 2 h in a humidified incubator at 37 °C. The loosely attached bacteria were rinsed off by dipping the substrates in a TSB solution. 4 – 6 parallel samples were placed in microcentrifuge tubes containing 1 ml of 0.5 wt% Tween 20 (Sigma-Aldrich) in TSB. In order to remove the cells from the substrate, the samples were sonicated for 5 min. The bacteria in the suspensions were plated with appropriate dilutions on tryptic soy agar plates and the colonies were counted after an overnight incubation.

A drop deposition method was used for studying bacterial adhesion on the printed cell study arrays (Paper 3). The cell study arrays were placed on a sterile petri dish and a 90 µl drop of the diluted *S. aureus* preculture was pipetted in the test area. After an incubation period of 2 h at 37 °C, the drops were removed by pipetting from the test area, and the test area was rinsed with 100 µl of ultrapure water by pipetting in order to remove the loosely

bound bacteria. The bacteria were counted as described for the static biofilm method above.

5.4. Surface characterization methods

5.4.1. Atomic force microscopy

Atomic force microscopy (AFM) is a technique belonging to the family of the scanning probe microscopy (SPM) that covers several techniques for probing a surface. AFM was introduced by Binnig et al. in 1986 [Binnig 1986], followed by the development of numerous applications [Fujihira 1999, Sahin 2008, Hardin 2011, Young 2011]. The wide range of operating modes and the variety of samples that can be investigated with AFM have made it the most used scanning probe microscope technique.

An AFM probe, consisting of a sharp tip in a nanometer scale, a flexible cantilever and a cantilever holder, scans over the sample surface that is moved by a piezoelectric xyz-scanner (Figure 10) [Hardin 2011]. The tip-sample interactions cause cantilever bending when the tip and the sample are brought close to each other. The deflection of the cantilever is determined with a laser beam that reflects from the end of the cantilever to the photodiode. The feedback loop between the optical detection system and the scanner generates the AFM images.

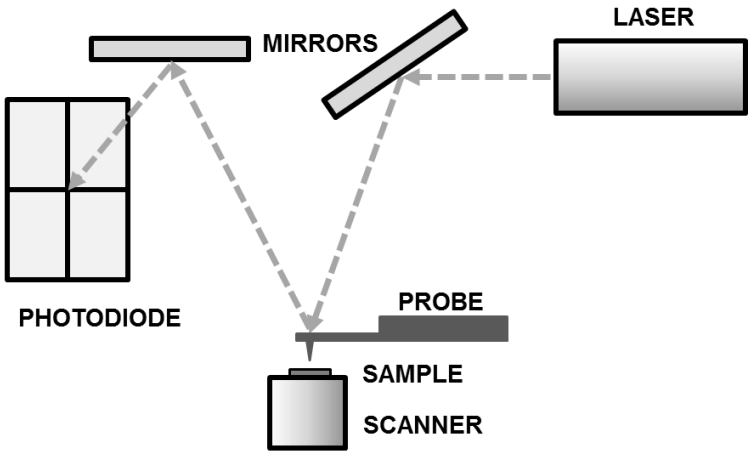

Figure 10. Configuration of an atomic force microscope.

In intermittent contact mode AFM (also called as tapping mode), the cantilever is oscillated at or close to its fundamental resonance frequency with predetermined amplitude, being excited by a piezocrystal in the cantilever holder [Hardin 2011, Zhong 1993]. As the tip approaches the surface, it begins to tap the surface during the oscillation cycles. The amplitude, resonance frequency and phase angle of oscillation change due to tip-sample interactions that include van der Waals and short-range repulsive interactions, and electrostatic, adhesion and capillary forces [Garcia 2002]. The amplitude is kept constant during the scanning by adjusting the tip-sample distance, and also in this system the photodiode-piezo unit feedback loop generates an AFM topograph of the surface. In comparison to contact mode AFM where the deflection of the cantilever is kept constant and the tip is continuously in contact with the sample, the risk for damaging the sample or contaminating the tip by the sample is decreased in the intermittent contact mode. Intermittent contact mode is thus a suitable AFM mode for examining soft samples, such as materials of biological origin.

The surface potential mode of AFM (SP-AFM) is an electric technique that uses a two-pass measurement in which the topography is detected during the first scan over the surface in intermittent contact mode, followed by scanning with a lifted tip at a constant tip-sample distance. The effective surface potential of the sample surface is measured during the second scan by adjusting the voltage on the tip to that of the sample. Samples consisting of regions of different materials show a contrast in a surface potential image due to the contact potential differencies [Hardin 2011]. In the case of molecular systems with dipoles, surface potential can be related to the strength and orientation of molecular dipoles [Fujihira 1999].

Torsional harmonic mode AFM (TH-AFM or HarmoniX^{TM}), also working in intermittent contact mode, gives information on several nanomechanical properties of the surface simultaneously with the topography and phase imaging [Sahin 2008, Sahin 2008b]. The torsional harmonic probe consists of a tip located at one side of a T-shaped cantilever, i.e. the tip is non-symmetrically positioned in the cantilever [Sahin 2007]. As the cantilever is oscillating vertically

over the surface at a higher harmonic frequency, a torsional movement is induced by the tip-sample interactions. Each oscillation cycle produces a force-distance curve (Figure 11) that is used to map the tip-sample interaction forces, such as adhesion force (F_{adh}).

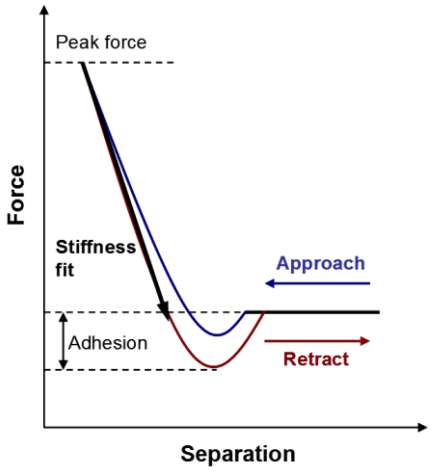

Figure 11. A force-separation curve.

Material properties of surfaces and tip-sample adhesion can be mapped also by PeakForce™ quantitative nanomechanical mapping (QNM™) (referred to as peak force AFM or PF-AFM in this work) that is based on measuring the force curves at a non-resonant mode [Young 2011]. The peak force can be accurately controlled with the force curves and by choosing an AFM probe with a suitable spring constant value. Using low peak force is beneficial for minimizing the damage or deformation of sensitive samples, such as proteins.

A common problem of the AFM measurements is the convolution effect arising from the shape of the tip that influences the lateral resolution of an AFM image, i.e. the lateral dimensions of imaged objects get distorted (overestimated). The cone angle and the radius of curvature (R) of the tip in addition to the radius of the imaged object (r) contribute to the tip-sample convolution, resulting in the observed (measured) lateral dimension r_c of the object according to

$$r_c = 2\sqrt{Rr} \qquad (12)$$

The convolution is most pronounced when the tip and the imaged object are of the same size range (Figure 12) [http://www.ntmdt.com].

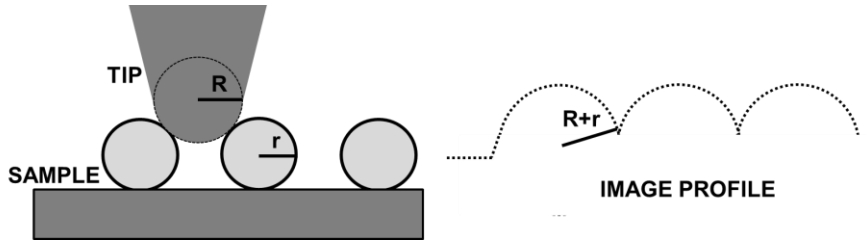

Figure 12. The convolution effect in the case where the radius of curvature of the tip is comparable to the dimensions of the imaged object (R ≈ r) [http://www.ntmdt.com].

In this work, all the AFM measurements were performed with intermittent contact mode in air, either alone or simultaneously with other AFM modes. The SP-AFM and the TH-AFM were used in Paper 1. The PF-AFM mode was used in Paper 3. NanoScope V MultiMode 8 AFM (Multimode^{TM}, Bruker) and NTegra Prima AFM (NT-MDT, Russia) were used as described in Papers 1 - 3. Roughness analyses were performed with the Scanning Probe Image Processor software (SPIP, Image Metrology, Denmark). Typically, the topographs were filtered with a Gaussian filtering and fitted by a LMS fit.

5.4.2. Contact angle measurements

The contact angle measurements and determination of the surface energy has been described in section 3.2. Static apparent contact angles were measured with a CAM 200 contact angle goniometer (KSV Instruments Ltd., Papers 1 - 3). The surface energy was determined in ambient conditions by using water (ultrapure MilliQ water), diiodomethane (DIM, Sigma) and ethylene glycol (EG, Sigma-Aldrich) as probe liquids with a typical drop volume of 1-2 µl.

5.4.3. X-ray photoelectron spectroscopy

X-ray photoelectron spectroscopy (XPS) is used to examine the elemental composition and the chemical state of atoms on surfaces [Kibel 2003, Briggs 1994]. A low sampling depth of XPS, ≤ 10 nm, makes it a very surface sensitive method. The sample surface is irradiated in ultra-high vacuum with X-ray photons that interact with the atoms located in the surface region causing emission of electrons from the core levels (photoelectrons) and from the valence levels (Auger electrons). The emitted photoelectron has a kinetic energy that is characteristic for the corresponding element. The different binding energies can be used to identify different atoms. The binding energy of the element can be calculated from the measured kinetic energy of the photoelectrons by

$$E_{binding} = hv - E_{kinetic} - W \quad (13)$$

where hv is the energy of the photons, $E_{kinetic}$ is the kinetic energy of the emitted electrons and W is the work function of the spectrometer. The binding energy is calculated in respect to the Fermi level of the solid, and the work function describes the energy difference between the vacuum level and the Fermi level.

In this work, the XPS spectra were obtained with a PHI Quantum 2000 scanning spectrometer at a measurement angle of 45°, using monochromatic Al Kα (1486.6 eV) excitation and charge neutralization. The atomic concentration of the elements was calculated by using the Multipak v 6.1A (Physical Electronics) software.

5.4.4. Quartz crystal microbalance

In quartz crystal microbalance (QCM), a piezoelectric quartz crystal with electrodes on both sides is oscillated at its resonant frequency by applying an electric field. QCM is a label-free in situ method that is used to detect the mass of adsorption via frequency changes. For sufficiently rigid films, the mass change, Δm, can be calculated according to the Sauerbrey relation (eq. 14) [Sauerbrey 1959]. For the validity of the Sauerbrey relation, the adsorbed layer should

also be thin and evenly distributed, and the adsorbed mass small compared to the mass of the crystal. The change of frequency is related to the adsorbed mass through

$$\Delta m = -\frac{C}{n}\Delta f_n \qquad (14)$$

where C is a mass sensitivity constant, f is frequency and n is the frequency overtone number.

QCM with dissipative monitoring (QCM-D) can be used to obtain the viscoelasticity of adsorbed materials by measuring the decay of oscillation [Rodahl 1995, Rodahl 1996, Rodahl and Kasemo 1996]. The energy applied during a QCM-D experiment decays faster for a non-rigid adsorbed film with viscoelastic properties, in comparison to a rigid or non-viscoelastic film. The dissipation factor, D, is reciprocal of the dimensionless Q factor (eq. 15) [Rodahl 1997, Vogt 2004].

$$D = Q^{-1} = \frac{R}{2\pi f L} = \frac{E_{dissipated}}{2\pi E_{stored}} \qquad (15)$$

where R is resistance, L is inductance, f is frequency, $E_{dissipated}$ is the dissipated energy and E_{stored} is the stored energy during one oscillation period.

QCM-D can be used to study the mass and the rigidity of adsorbed protein layers. The detected mass includes both the mass of the adsorbed component and the mass of water that is entrapped within the adsorbed layer [Bingen 2008, Ray 2015]. For example, the layer of avidin that does not saturate the surface may contain up to 86 m-% of water whereas a protein layer with a saturated coverage could still contain 50 m-% of water.

In this study, the protein adsorption experiments were made with an impedance based QCM-D equipment (QCM-Z500, KSV Instruments, Finland) with a batch sampling measurement chamber at a constant temperature of 25 °C (Papers 1 and 3). The volume of the measurement chamber is approximately 300 µl. The QCM measurement chamber was first filled with buffer and when a stable baseline was achieved, solutions of interest were dosed into the measurement chamber via a temperature loop. The chamber was flushed with buffer between each addition of the sample solution in order to remove any excess or unspecifically

bound protein. The surface titrations with avidin were conducted by alternating the avidin solutions with an increasing concentration and buffer (Paper 3). The frequency and dissipation changes were monitored and, accordingly, the adsorbed mass and rigidity of the adsorbed layers were evaluated.

6. SUMMARY OF THE RESULTS

The work was initiated by characterizing different substrates to be used for protein adsorption and cell growth studies. Paper substrates with latex coatings were found to support the cell growth best compared to the other paper coating materials. Latex coatings were thus further developed. Latex surfaces were IR treated and the surface chemistry and topography were modified by changing the coating composition. These coatings were used for protein adsorption and patterning studies with three model proteins. Moreover, the printability of proteins and cells was demonstrated with the developed latex surface as a printing substrate. The conformation and activity of avidin on the latex surface were examined. Finally, the cell study platform without and with pre-adsorbed avidin was used to study the bacterial adhesion.

6.1. Surface properties of the studied substrates

The surface properties of pigment-coated (Paper 2) and latex-coated (Papers 1 and 3) paper substrates are summarized here. Latex blends were rod-coated on precoated paper substrates, as described in section 5.1.1. The effect of IR treatment on the composition, topography and energetics of the latex coatings, in comparison to the pristine latex surfaces, was first studied (Paper 1). The surface properties of the IR treated coatings were then modified by changing the composition of the latex blend (Paper 3). The surface properties of the PS slides modified with PLL and plasma treatment are also described in this chapter. The PS slides were used as substrates for printing and analyzing the viability of ARPE-19 and HepG2 cells (unpublished data).

6.1.1. Composition of pristine and IR treated latex coatings

Pristine single-component ABS latex coatings consisted of an ordered lattice of latex particles with a diameter of 135 – 170 nm, according to the AFM measurements (Figure 13 a). The PS coatings differed from the ABS coatings in that the PS particles were more randomly packed, presumably as a result of more polydispersed particles (diameter 90 – 190 nm) (Figure 13 c). Both ABS and PS particles were deformed in the vertical direction in the coating (Figure 13 b and d), i.e. flattened, whereas the measured lateral diameter of the particles in the coating corresponded to the size of the particles in the dispersion (140 nm) [Ihalainen 2010, Steward 2000]. The flattening was more pronounced for the ABS particles due to the lower glass transition temperature (T_g) that enabled the drying of the coating to proceed to the film formation stage. The S_q values decreased from 2.9 nm (pristine) to 0.5 nm for ABS and from 23 nm to 1.3 nm for PS due to the IR treatment.

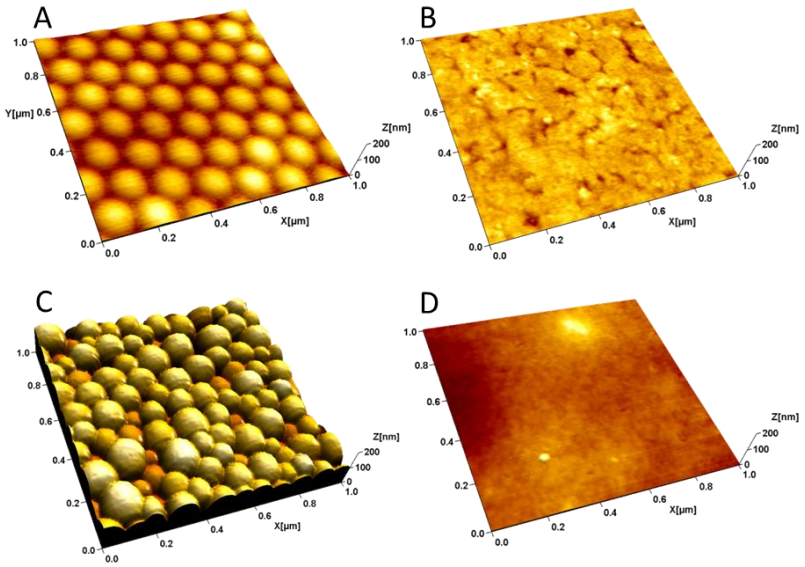

Figure 13. AFM topographs of the pristine single-component ABS latex coating (a), the IR treated single-component ABS coating (b), the pristine single-component PS latex coating (c) and the IR treated single-component PS latex coating (d). The image size is 1 µm × 1 µm.

Surfactants based on sodium salts of anionic sulfate or sulfonate are commonly used in latex dispersions in order to keep the dispersions stable [De Haenen 2004, El-Aasser 1983]. The drying of the latex coating induces the migration of the surfactants to the surface [Backfolk 2006]. In this study, sulphur and sodium were detected with XPS, which was attributed to the presence of surfactant molecules on the surface (Table 2). Lower relative amounts of sulphur and sodium in the PS coating in comparison to the ABS coating (Table 2) indicates that the coatings had proceeded to different stages of drying. The ABS coating had presumably proceeded to the film-forming stage (final drying stage), whereas the drying of the PS coating had not proceeded equally far (Figure 13 a and c). Sulphur may also originate from persulfate initiators used in the emulsion polymerization [Van den Hul 1970].

The presence of oxygen can originate from the surfactants and, additionally, from the carboxyl groups on the carboxylated ABS latex. Although there are nitrile groups in the ABS polymer chains, the XPS measurements of the pristine latex surfaces did not show any nitrogen, which indicates that the ABS film was at least partly covered by surfactants (Paper 1). The surfactants on the surface naturally modify the surface energy, and for the pristine ABS surface a low $\theta_{w,a}$ value was observed (Table 2).

The pristine two-component latex coating consisted of locally clustered particles partially embedded in the continuous film (Figure 14 a). As discussed earlier, the low-T_g ABS latex forms a film already at room temperature, thus the observed particles represent the high-T_g PS latex intermixed with the continuous ABS film. The surface elemental composition of the pristine two-component latex coating was quite similar to that of the ABS coating, although with less sodium and sulphur due to the increased surface coverage of PS (Table 2).

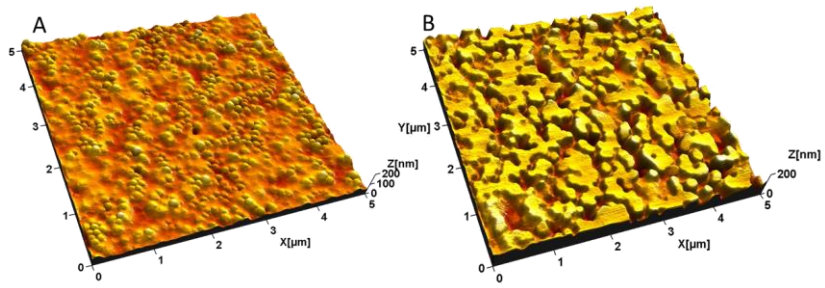

Figure 14. AFM topographs for the pristine (a) and the IR treated (b) two-component ABS/PS latex coating with PS:ABS weight ratio of 40:60. The image size is 5 µm × 5 µm.

Table 2. Surface analysis data for the pristine and IR treated ABS and PS latex coatings. Data for elemental composition by XPS, apparent water contact angle ($\theta_{w,a}$), surface energy (γ) and tip-surface adhesion force (F_{adh}) values is included. Papers 1 and 3.

XPS elemental composition [at%]

Paper 1						
Treatment	**Phase**	**C1s**	**O1s**	**Na1s**	**S2p**	**N1s**
Pristine	PS	91.3	6.2	1.3	0.5	
IR treated	PS	96.8	2.8	0.4		
Pristine	ABS	69.8	19.8	7.1	3.4	
IR treated	ABS	76.9	15.3	5.0	2.8	
Pristine	PS, ABS	76.1	18.2	3.1	1.9	
IR treated	PS, ABS	93.6	6.4			
Paper 3						
Treatment	**Phase**	**C1s**	**O1s**	**Na1s**	**S2p**	**N1s**
IR treated	ABS	94.1	5.8			0.5
IR treated	85 % PS	95.3	4.7			

Apparent water contact angle ($\theta_{w,a}$)

Paper 1		
Treatment	**Phase**	**$\theta_{w,a}$ [°]**
Pristine(*	PS	90 ± 2
IR treated(*	PS	86 ± 3
Pristine(*	ABS	31 ± 2
IR treated(*	ABS	45 ± 3
Paper 3		
Treatment	**Phase**	**$\theta_{w,a}$ [°]**
IR treated(**	PS	98 ± 3
IR treated(**	ABS	66 ± 3

Surface energy (γ)

Paper 3					
Treatment	**Phase**	**Surface energy [mN/m]**			
		γ^{LW}	γ^{+}	γ^{-}	γ^{tot}
IR treated	PS	43.6	0.0	0.0	43.6
IR treated	ABS	39.8	0.0	7.1	40.1

Tip-surface adhesion force at zero peak force (F_{adh})

Paper 1		
Treatment	**Phase**	**F_{adh} [nN]**
Pristine	PS	3.9 ± 0.4
IR treated	PS	1.9 ± 0.2
Pristine	ABS	3.5 ± 0.3
IR treated	ABS	2.1 ± 0.2

The surface structure and chemistry were modified by the IR treatment and the subsequent rinsing step. The single-component latex coatings formed films that smoothened during the IR treatment. The film formation and particle coalescence were enabled by the autohesion, i.e. the inter-particle migration of the polymer chains, initiated by the IR treatment [Steward 2000].

When the two-component pristine latex coating was IR-treated, the resulting surface comprised two height levels representing the two latex components (Figure 14 b). The higher level corresponds to PS that appears as randomly shaped and flattened clusters of PS. These clusters were partially embedded in the lower level phase attributed to the smooth ABS film. Surface topography of the two-component latex showed a drastic change after the IR treatment and, contrary to the single-component coatings, the surface roughness increased. Surface topography of the two-component latex coatings is discussed in more detail in section 6.1.2.

The $\theta_{w,a}$ value of the single-component PS latex either remained approximately the same (Paper 1) or increased (Paper 3) as a result of the IR treatment, and also the IR treated PS had the hydrophobic characteristics. The $\theta_{w,a}$ value for the single-component ABS latex surfaces increased but remained in the hydrophilic region. The hydrophilicity of ABS was expected due to the carboxylation of the ABS latex. The sulphur and sodium surface content of the ABS phase decreased (Paper 1) or disappeared completely (Paper 3, Table 2).

The surface of the IR treated two-component latex films consisted of carbon, oxygen and nitrogen (Paper 3). High resolution nitrogen spectra showed a linear decrease with increasing surface ratio of the hydrophobic latex, suggesting the removal of surfactants and indicating that the nitrogen content indeed results from the nitrile groups of the ABS latex component. Thorough rinsing was a crucial step for removal of the sulphur and sodium containing additives during this study. The differencies in the surface characteristics between the latex coatings in Paper 1 and Paper 3 are mainly due to the improved rinsing procedure in Paper 3.

Surface energy calculations for the IR-treated single-component surfaces (Paper 3, Table 2) showed that γ^{tot} is slightly higher for the apolar PS, whereas ABS films showed a Lewis basic character, γ^-. The nitrile groups of ABS can be considered to have relatively strong Lewis basic nature with pK_a of about 24 [Bordwell 1978]. The Lewis basic nature can be attributed to the enhanced attractive interaction between bipolar materials and the surface [Chibowski 2000, Li 2004, van Oss 1987].

The adhesion force, F_{adh}, between the AFM tip and the sample was measured for pristine and IR treated two-component latex (Paper 1, Table 2). The F_{adh} values were extrapolated to the zero peak force value in order to minimize the influence of tip indentation. The IR treated sample showed lower F_{adh} values than the pristine sample. On the other hand, only a small difference was detected between the PS and the ABS phases. The tip-sample adhesion could be attributed to the van der Waals interactions, since the contribution of chemical bonding and electrostatic interactions to F_{adh} could be assumed to be negligible. The chemical bonding between the tip and the sample is unlikely and the silicon tip surface is not expected to accumulate surface charges. The decreased value of F_{adh} after the IR treatment may indicate the removal of the surfactants that, with their polar nature, are expected to increase the tip-sample interactions.

The surface potential values were also measured for the IR treated ABS and PS phases with AFM (about -540 mV and -600 mV, correspondingly), and their change after the contact with a protein solution was further related to the protein adsorption (Paper 1).

6.1.2. Influence of the latex blend composition on surface topography

The weight ratio of hydrophobic PS and hydrophilic ABS in the latex blend was changed in order to modify the surface topography and chemistry of the latex coating (Paper 3). The smooth film-like surface of the ABS coating evolved towards a structured surface with two height levels, when the amount of PS was increased in the coating blend (Figures 15 and 16). The height distribution was clearly bimodal with a height difference of 20-40 nm between the

two distinct height levels. The relative surface coverage of PS increased linearly with a slope of 1.37 up to 60:40 weight ratio of the PS component in the latex blend and, due to this, the surface topography could be tailored in a controlled way.

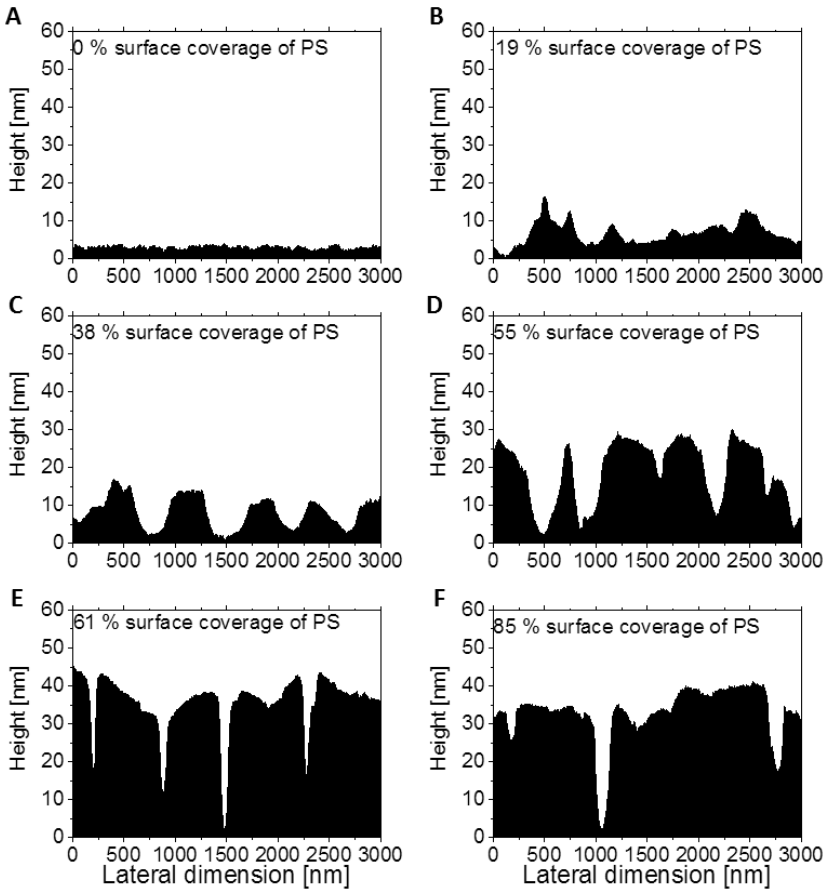

Figure 15. Height profiles of the latex surfaces with varying surface coverage of the PS component. The increasing values of surface coverage of PS correspond to the PS:ABS weight ratios (wt%) of a) 0:100, b) 20:80, c) 30:70, d) 40:60, e) 50:50 and f) 60:40 in the blend, respectively. Paper 3.

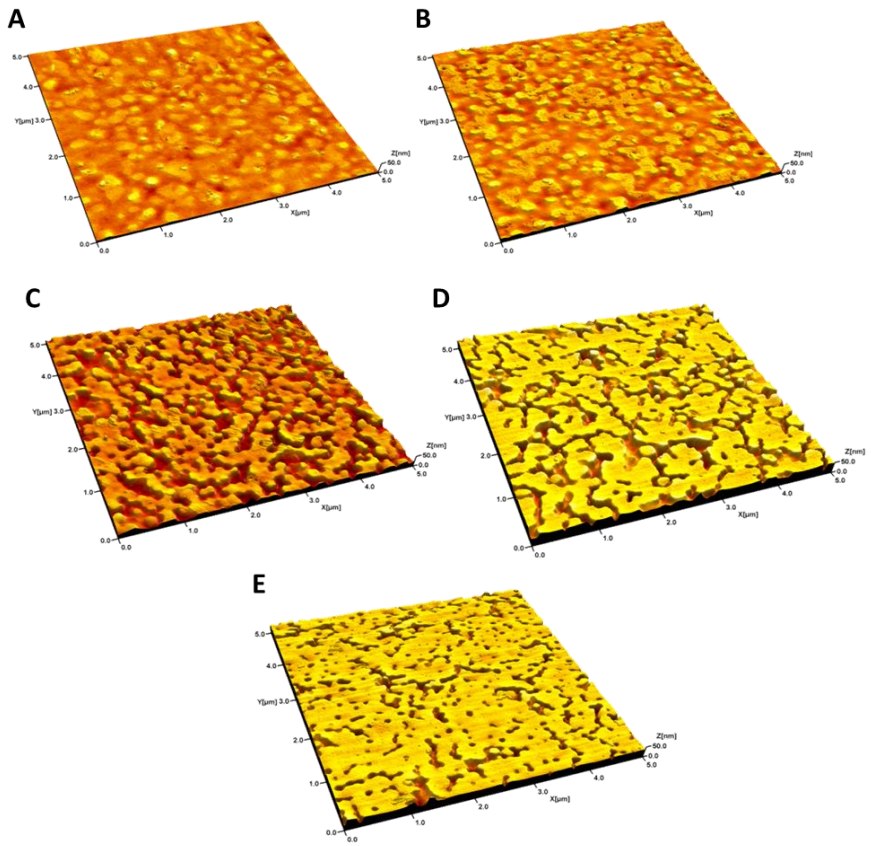

Figure 16. AFM topographs of the latex surfaces with varying surface coverage of the PS component. The increasing values of surface coverage of PS correspond to the PS:ABS weight ratios (wt%) of a) 0:100, b) 20:80, c) 30:70, d) 40:60, e) 50:50 and f) 60:40 in the blend, respectively. Paper 3.

Roughness of the latex coatings was analyzed from the AFM topographs of 5 µm × 5 µm and 150 nm × 150 nm. In the smaller scale, the roughness values of both latex components remained unchanged regardless of the coating composition (Table 3). In the larger scale, S_{dr} (increment of the interfacial surface area) and V_v (total void volume) roughness increased as a function of the relative surface coverage of the PS phase up to 61 % surface coverage of PS (Figure 17). S_{dr} may contribute to the loading capacity of the surface. The higher V_v value indicates both poorer bearing characteristics and better fluid retention of the surface

and, if the size of the adsorbate is large enough, V_v can be related to the contact area between the surface and the adsorbate.

Table 3. S_{dr}, S_q and S_{cl} roughness values for ABS and PS latex phases. The roughness parameters are calculated from 150 nm × 150 nm AFM topographs. Paper 3.

	S_{dr} [%]	S_q [nm]	S_{cl} [nm]
ABS	0.8 ± 0.2	0.55 ± 0.16	20 ± 4.5
PS	0.5 ± 0.1	0.71 ± 0.09	10 ± 2.1

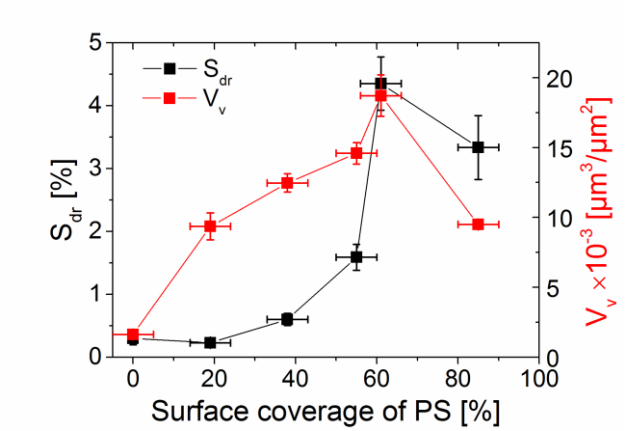

Figure 17. Surface area ratio (S_{dr}) and total void volume (V_v) for the composite latex surfaces versus surface coverage of the PS phase. The roughness parameters are calculated from 5 µm × 5 µm images. Paper 3.

In conclusion, IR treatment together with the rinsing step caused the decrease or removal of the additives from the surface. Furthermore, the IR treatment resulted in the coalescence of the PS particles and in the formation of a bimodal topography with two distinct height levels, the higher level representing hydrophobic PS and the lower level representing the hydrophilic ABS layer.

6.1.3. Surface properties of pigment coatings

The AFM topographs for the pigment coatings are shown in Figure 18. In Table 4, the water contact angle values, the surface energy

values, and the roughness parameter values for these surfaces are listed.

The PCC surface had the lowest bearing area and the highest S_q and S_{dr} values. The apparent water contact angle of the PCC coating was very close to 90˚, being thus practically a non-wetting surface. The kaolin surfaces were found to be partially wetting, the two-component kaolin surface having the most water wettable nature with the highest Lewis basic and polarity values. The kaolin coatings had S_{dr} values close to each other, whereas the one-component kaolin surface showed a higher S_q value and a bearing area ratio value. For comparison, the two-component latex with 55 % surface coverage of PS had the bearing area ratio value of 74 ± 5, similar to that of the one-component kaolin coating (Paper 2).

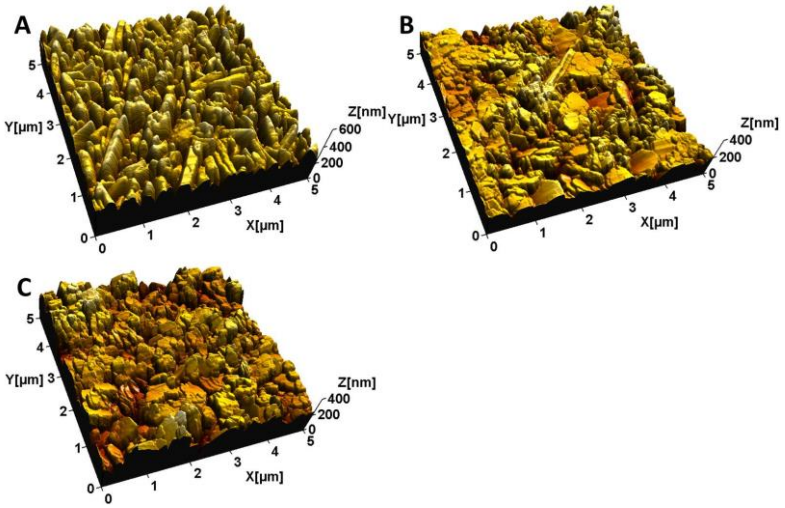

Figure 18. AFM topographs of a) a PCC coating, b) a coating with two different kaolin pigments, and c) a one-component kaolin coating. Paper 2.

Table 4. Apparent water contact angle ($\theta_{w,a}$), surface energy (γ), and roughness parameter values for the pigment coatings. Paper 2.

Apparent water contact angle ($\theta_{w,a}$)

Pigment coating	**$\theta_{w,a}$ [°]**
PCC	87 ± 3
Two-component kaolin	15 ± 3
One-component kaolin	56 ± 2

Surface energy (γ)

Pigment coating	**Surface energy [mN/m]**				
	γ^{LW}	**γ^{+}**	**γ^{-}**	**γ^{tot}**	**Polarity [%]**
PCC	31.6	0.6	1.3	33.3	5.1
Two-component kaolin	27.2	1.3	20.5	37.5	27.5
One-component kaolin	34.5	0.3	8.6	37.5	8.0

Roughness parameters

Pigment coating	**Roughness parameters**		
	Bearing area [%]	**S_q [nm]**	**S_{dr} [%]**
PCC	29 ± 5	76 ± 4	42 ± 9
Two-component kaolin	60 ± 15	36 ± 3	26 ± 2
One-component kaolin	76 ± 13	50 ± 10	25 ± 3

6.1.4. Surface properties of the P-PLL-PS slides

PS microscopy slides were used as substrates for the cell printing tests. A modification of the surface was needed in order to achieve good print quality in the printing tests with matrigel (Table 5). Positively charged PLL is widely used as a coating material for an improved cell-surface interaction [Morga 2015]. Here, the surface treatment of the PS slide by PLL and plasma was carried out in order to enhance the wettability of the surface. Indeed, the PS slide coated with PLL had a much smaller θ_W than that of the nontreated PS slide. The hydrophilicity of the PLL-coated PS slide was further increased with the plasma treatment (P-PLL-PS),

mainly through increased roughness of the surface. An even matrigel layer (visual inspection) could be screen-printed on P-PLL-PS that was chosen for the cell printing experiments.

Table 5. S_{dr} values (from 5 µm × 5µm topographs), apparent water contact angles (θ_a) and Young contact angles (θ_Y; calculated by using eqs. 4 and 5) for the PS slides without surface treatment and with PLL and plasma treatments. Unpublished data.

Substrate	S_{dr} [%]	θ_a [°]	θ_Y [°]
PS	10.3	87±1	87
PLL treated PS (PLL-PS)	3.0	47±2	49
PLL and plasma treated PS (P-PLL-PS)	14.5	6±1	30

6.2. Protein adsorption on the latex coatings

The characterization of the different latex coatings showed that surfaces with both different chemical and topographical properties can be prepared by varying the composition of the coating. The next step was then to study how proteins adsorb to these different latex surfaces. The coatings were expected not only to offer a substrate for protein immobilization but also for creating patterned structures. The immobilization was examined for bovine serum albumin (BSA), fibronectin (FN) and streptavidin (SA) (Paper 1). Furthermore, the adsorption of avidin to the hydrophobic PS and hydrophilic ABS latex phases was studied in Paper 3. The activity of adsorbed streptavidin was verified by using biotinylated CRP antigen (Paper 1).

6.2.1. Influence of surface chemistry and topography on protein immobilization

Adsorption of BSA, FN and SA was studied with XPS, surface topography measurements (AFM), surface potential AFM and QCM. BSA adsorbed readily to the PS and ABS phases, both on the

pristine and the IR treated surface, despite their different surface chemistry. A structurally flexible BSA protein contains both hydrophilic and hydrophobic domains, as well as charged and uncharged regions, which enables adsorption to many types of surfaces [D´Sa 2010]. At the adsorption pH of 7, the overall surface charge of BSA (IEP 5) is, however, negative. BSA was found to adsorb to the pristine surface containing anionic surfactant molecules, which indicated that the overall electrostatic interactions may not have dominated the adsorption of BSA [Jeyachandran 2009]. BSA is able to undergo structural changes during the interaction with the surface, leading to enhanced adsorption ability.

Contrary to BSA, the adsorption of FN and SA to the pristine surface was smaller or almost fully inhibited. FN had negligible adhesion toward the pristine surface, whereas it appeared in globular-like form on the PS phase of the IR treated coating. Also SA adhered preferentially to the PS phase of both the pristine and the IR treated surfaces. However, only a small amount of streptavidin adsorbed, partly reversibly, to the pristine surface compared to the IR treated latex surface, as evident from the QCM measurements.

Enhanced protein adsorption to the hydrophobic PS phase was expected. Suppressed protein adsorption to the ABS phase most probably resulted from the hydrophilicity of this phase and the increased polymer chain mobility of ABS, as it is in the amorphous state at room temperature [Liu 2009, Ji 2000, Otsuka 2004]. The electrostatic interactions between the charged proteins and the surface were also suggested to affect the protein adsorption. At pH 7, the net negatively charged FN experienced electrostatic repelling forces toward the negatively charged pristine surface [Österlund 1988, Belegrinou 2008]. The electric double layer interactions of the near-neutral SA protein are suppressed at pH 6–7.5 [van Oss 2003 b]. Thus the used buffer solution and the hydrophobic interactions take the main role in the adsorption process [van Oss 1993, Kidoaki 1999]. Due to the different surface chemistry of the PS and ABS phases, the IR treated two-component latex surface enabled patterned adsorption of fibronectin and (strept)avidin.

The avidin adsorption experiments were performed for various protein concentrations on the IR treated latex coatings (Paper 3). Avidin patterning on the IR treated surface was observed at low concentrations of 0.35 and 3.5 µg/ml (Figure 19), whereas higher concentrations did not give any F_{adh} difference between the two latex phases. At higher concentrations, avidin adsorbed to both of the latex phases and, as a result, the F_{adh} difference disappeared.

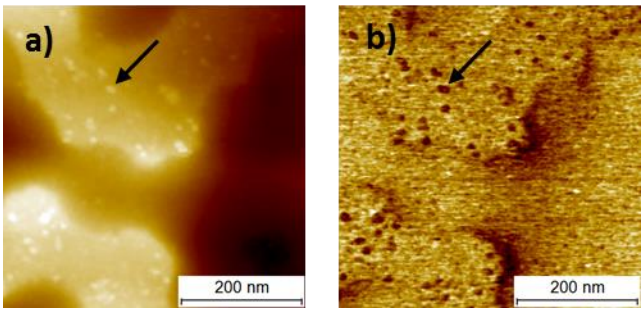

Figure 19. An AFM topography image (a) and an adhesion force (F_{adh}) map (b) on avidin molecules at a two-component IR treated latex surface adsorbed from a solution of concentration 0.35 µg/ml. The arrows point to avidin adsorbed to the PS phase. In the F_{adh} map, the darker contrast indicates a lower tip-sample adhesion force. Unpublished data.

The morphology of adsorbed avidin changed from single and separated protein molecules towards a mesh-like structure with increasing concentration (Figure 20). On the PS phase, the average height of the adsorbed proteins varied between 3 and 5 nm, which compares well to the dimensions of an avidin tetramer (4 × 5.5 × 6 nm). A smaller height value (2 – 3 nm) was detected for avidin on the surface of ABS. The S_{dr} roughness values for the surfaces with immobilized avidin increased with the concentration on both of the latex phases, the increase being more pronounced on the PS phase. A maximum was found at the concentration of 10 µg/ml. In the AFM measurements, however, the tip convolution effect limits the detection accuracy of the lateral dimensions of the objects in the protein layers. Therefore, the degree of surface coverage of the avidin layer could not be reliably determined from the AFM topographs.

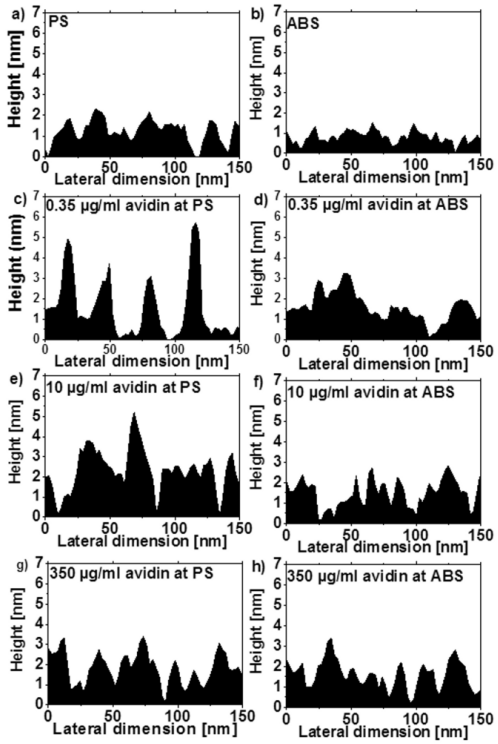

Figure 20. Line profiles (from 150 nm × 150 nm AFM topographs) over the PS phase (a, c, e, g) and the ABS phase (b, d, f, h) before and after avidin immobilization from different concentrations as indicated in the profile images. Paper 3.

In addition, AFM topographs showed occasional double layer structures for films being deposited from solutions with concentrations above 10 µg/ml (Figure 21). These double layer structures were mainly observed on the PS phase. The thickness of the upper layer in the double layer structure was generally higher than the monolayer avidin film on the PS phase, being 5-6 nm. The conformational changes, i.e. the surface-induced denaturation, of the protein layer adsorbed on the hydrophobic surface have been shown to induce a stronger protein-protein interaction, resulting in agglomeration of protein molecules [Kamiya 2014], which could explain the double layer formation on PS.

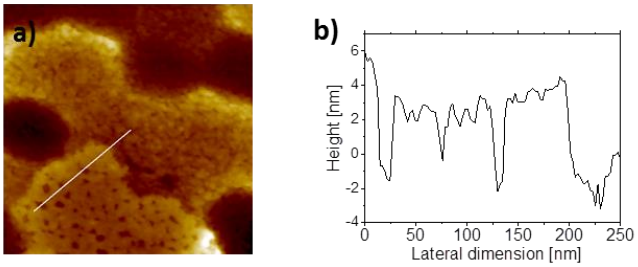

Figure 21. An AFM topograph (image size 500 nm × 500 nm) and a height profile of an avidin double layer on a two-component latex surface. Avidin was adsorbed from a solution with 100 µg/ml concentration. The dark/light color contrast refers to low/high topographical features. Unpublished data.

The QCM measurements showed that the two-component latex surface became almost saturated at an avidin concentration of about 100 µg/ml (Paper 3). A minor decrease of the frequency was observed when the sample surface was rinsed with the buffer only after adding the high concentration (100 µg/ml or 350 µg/ml) solution of avidin to the QCM chamber. Additionally, avidin was observed on the paper coatings after vigorous rinsing with water, as observed by AFM and XPS (Paper 3). This indicates that the protein-surface interaction was relatively strong and irreversible, which would allow the use of the substrate in applications based on avidin-biotin functionality.

The avidin loading capacity of the latex coatings at the saturation concentration regime (350 µg/ml) depended on the composition of the surface. When the relative surface coverage of the PS phase was increased from 0 % to 85 %, the effective mass of the adsorbed avidin increased by 25 % (Figure 22). This is in accordance with the general observation of hydrophobic surfaces having a higher protein loading capacity than hydrophilic surfaces (section 4.1.). Additionally, the ordered and disordered regions of proteins and their multi-domain structure may affect the orientation of the adsorbed proteins, depending on the surface properties such as wettability (section 4.2.). The avidin molecules were suggested to obtain a different conformation and packing density on the ABS and PS phases (Paper 3). Previously, avidin has been shown to adsorb more tightly-packed on hydrophobic

surfaces and occupy a larger surface area on hydrophilic surfaces [Albers 2012, Vikholm-Lundin 2012]. Adsorption with side-on orientation to the hydrophilic ABS phase and adsorption with end-on orientation to the hydrophobic PS phase could also explain the higher packing density of avidin on PS. Avidin has shown to adopt a side-on orientation by binding specifically to carboxylated surfaces, although non-specific adsorption could lead to random orientation [Misawa 2006].

Furthermore, the increased surface area (S_{dr}) and the larger amount of interphases of chemically different material domains have previously been suggested to contribute to an increased protein loading capacity [Riedel 2001, Sutherland 2001, Kumar 2008, Dupont-Filliard 2004]. Here, the S_{dr} value increased only a few percentages with increasing surface coverage of PS (Figure 17), and thus can explain only partly the increased avidin adsorption.

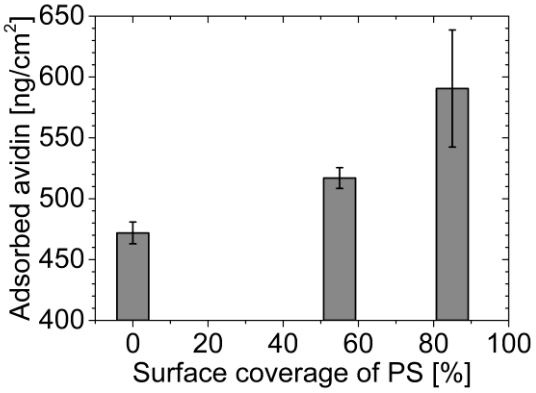

Figure 22. Adsorption of avidin to the ABS latex and two-component latex surfaces. Paper 3.

6.2.2. Activity of immobilized strept(avidin)

The specific binding activity of avidin to biotin-BSA was studied on IR treated latex surfaces as a function of increasing surface coverage of PS (Paper 3). Avidin was immobilized from a solution with a concentration of 350 µg/ml (Figure 22) in order to, firstly, ensure the surface saturation and, secondly, to minimize the denaturation of avidin [Vogler 2012, Seigel 1997]. The best specific

binding activity was detected on ABS where avidin bound 1.95 biotin-BSA molecules, whereas 1.27 – 1.45 biotin-BSA molecules were bound by immobilized avidin on the two-component latex surfaces (Figure 23). Surface-induced denaturation of avidin caused by the hydrophobic interactions was suggested to reduce the specific activity on the PS phase. The larger specific binding ability of avidin on ABS could be attributed to the lower packing density that allows avidin to bind two biotin molecules. The dense packing of avidin on the PS phase could have caused steric hindrance for binding of biotin-BSA.

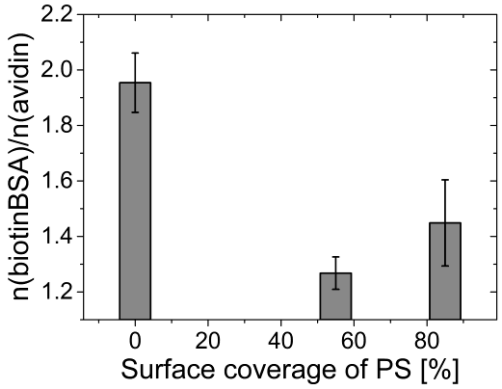

Figure 23. The molar binding capacity of biotin-BSA to pre-adsorbed avidin. Paper 3.

Furthermore, immobilized streptavidin was able to bind biotinylated CRP antigen (Paper 1). This was demonstrated for streptavidin that was adsorbed in the QCM chamber and, in addition, for ink-jetted streptavidin (Paper 1). (Strept)avidin is known for its structural stability [Huang 1994]. In this study, the biotin binding ability of streptavidin remained even after the printing and immobilization due to its stability upon adsorption. Ink-jetting enables high-throughput dispensing of proteins and could thus allow fast preparation of avidin-coated substrates for use in (strept)avidin technology.

6.3. Cell study platforms

The applicability tests of the paper-based 2-D platform for cell studies (Figure 9) were performed with three case studies: growth of pipette seeded epithelial ARPE-19 cells (Paper 2), growth and viability of printed HepG2 and ARPE-19 cells (unpublished data), and adhesion of *S. aureus* bacteria (Paper 3).

6.3.1. Epithelial cell growth and printability

Adhesion of ARPE-19 cells to four different coatings with characteristic topography and surface energy was studied (Paper 2). PCC, two-component kaolin, one-component kaolin, and two-component latex were used as coating materials on paper substrates.

Among the paper coatings, the two-component latex surface (55 % surface coverage of PS) supported the ARPE-19 cell growth most efficiently. After an incubation time of 48 h, the cells grew to 90 % confluency on the latex surface. On this surface, the confluency was 100 % after 72 h of incubation. The roughness values (S_q and S_{dr}) of the latex coating were the lowest compared to the other paper coatings, whereas the bearing area was relatively high. The Lewis basic character (7.8 mN/m) was in between the highest and the lowest values among the different coating surfaces.

Pigment coated papers showed varied supporting properties for the ARPE-19 cell growth. No cells were observed on the PCC coating. The PCC surface had sharp surface features and a grooved surface compared to the other substrates, resulting in a low bearing area and high S_{dr} and S_q values. Epithelial cells have been previously found to adhere more preferably to smooth surfaces than to rough surfaces [Baharloo 2005]. Moreover, their protrusion to narrow grooves has been shown to be prevented [Teixeira 2003]. This could lead to a reduced cell-substrate contact causing disturbed early focal contact, which has been found to inhibit the growth of ARPE-19 cells [Lim 2004].

The cell confluency was 7 % on the two-component kaolin and 42 % on the one-component kaolin surfaces after 48 h of incubation.

After 72 h incubation, ARPE-19 cells formed isolated clusters on the two-component kaolin surface, and grew to almost full confluency on the one-component kaolin coating. The S_{dr} values for these substrates were almost similar. The difference in the cell growth supporting nature between the two kaolin surfaces was related to the differences in the surface chemistry more than to the topography. The two-component kaolin surface had a significantly higher Lewis basic value, polarity and water wettability than the one-component kaolin surface. Within the surface properties of all of the paper coatings, low S_{dr} roughness, high bearing area and an intermediate Lewis basic character of the surface were found to be beneficial for adhesion and growth of epithelial ARPE-19 cells.

Cells were directed by cell-repellent PDMS to adhere and grow on the designed test areas (Figure 24). The growth of the pipette seeded ARPE-19 cells was supported by the two-component latex coating on the test areas, whereas the cells did not grow on the surrounding PDMS surface. Cell imaging was successful with an appropriate dye (DiO) emitting green light, because in this wavelength region the autofluorescence of paper is sufficiently low. Furthermore, lipophilic DiO did not stain the latex surface, and the cell membrane could thus be seen on the test areas. On the other hand, DiO adsorbed to the PDMS, causing fluorescence also on the areas surrounding the test areas. The cells could, however, be observed and distinguished due to their characteristic morphology and heterogeneous structure compared to the smooth PDMS surface.

The PDMS surface has very low surface energy which, with the high polymer chain mobility, resulted in a resistance towards biomolecule adsorption [Liu 2009, Ji 2000]. The low bacterial adhesion to PDMS compared to the paper coatings is further evidenced by the very low bacterial viable counts (discussed in section 6.3.2).

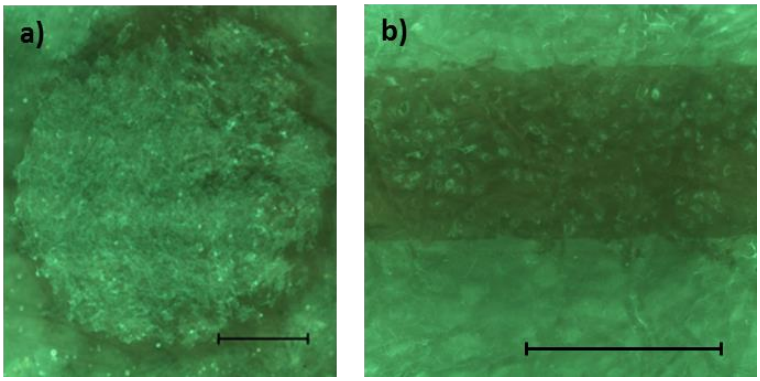

Figure 24. Cell directing by printed PDMS on a latex coating. The ARPE-19 cells were seeded with a pipette to substrates with a) circular test areas (Paper 2) and b) 2-D channels (unpublished data). The length of the scale bar is 500 µm.

The screen-printing method was an alternative approach for the pipette seeding in order to deposite the cells in matrigel to the cell study platform. This approach is described in section 5.3.1. Other hydrogel alternatives such as alginate and nanofibrillated cellulose have also been used successfully as 3D scaffolds for HepG2 cells [Bhattacharya 2012, Jeon 2016]. Here, the ARPE-19 and HepG2 cells were screen-printed in a matrigel mixture on the plasma treated and poly-L-lysine coated polystyrene (P-PLL-PS) microscope slides and the viability of the printed cells was followed for 72 hours (Figure 25, unpublished data). Both cell lines were found to be viable for 72 h, however, the HepG2 cells proliferated and showed high fluorescence intensity, whereas the ARPE-19 cells showed only a minor increase in the viability in comparison to the negative control during this time interval.

HepG2 cells were further screen-printed in matrigel on a paper substrate and the cells were viable within the incubation time of 72 h. However, the viability remained at the same level between 24 h and 72 h (Figure 25). The screen-printed HepG2 cells were also stained and imaged (Figure 26). On the P-PLL-PS substrate, the micrographs of screen-printed HepG2 showed a clear increase in the cell number. HepG2 cells on paper showed a more heterogeneous distribution after 72 h of incubation, in comparison to the incubation time of 24 h.

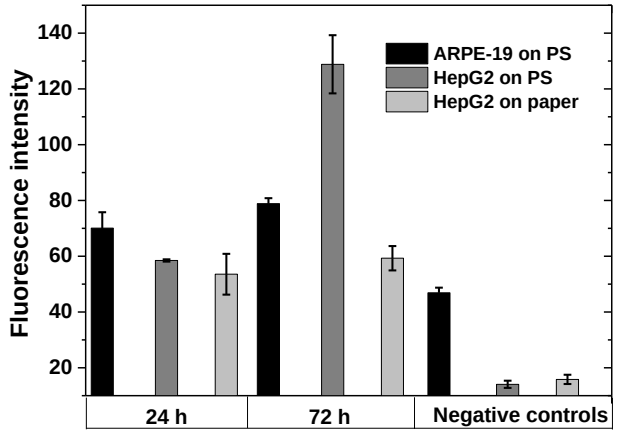

Figure 25. Viability of printed ARPE-19 and HepG2 cells on P-PLL-PS and paper (Alamar blue). Unpublished data.

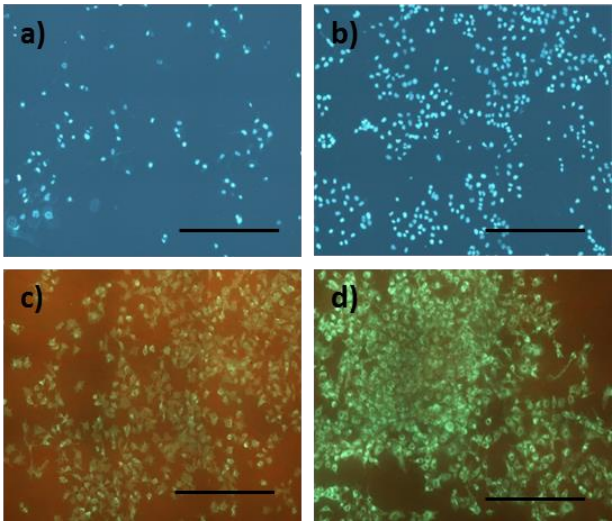

Figure 26. Nuclei of HepG2 cells printed in MG on P-PLL-PS (a and b) and the membranes of HepG2 cells printed in MG on two-component latex coated paper (c and d). The cells were incubated for 24 h (a and c) and 72 h (b and d). The nuclei of the cells on P-PLL-PS were stained with Hoechst and the cell membranes on paper were stained with DiO. The length of the scale bars is 500 nm. Unpublished data.

The printed ARPE-19 and HepG2 cells maintained their viability and ability to divide after the printing process. The screen printing method could, therefore, be used for transferring cell-containing biomaterial ink to various substrates. Other printing technologies such as laser-assisted bioprinting and ink-jet bioprinting have been utilized for transferring living cells with good precision, but a drawback is that they are time-consuming methods [Guillotin 2011, Calvert 2007]. As a high-throughput method, screen printing would allow scaling up of biofabrication processes.

6.3.2. Bacterial adhesion

The viability of *S. aureus* cells on the different latex surfaces, PDMS and glass was quantified by the bacterial viable counts (Figure 27, Paper 3). The latex surfaces were either uncoated or coated with avidin.

The bacterial adhesion increased slightly with the higher surface coverage of the hydrophobic PS phase and a larger effective surface area. The hydrophobic interactions and the increased roughness have been shown to enhance the adhesion of *S. aureus* [Müller 2007, Tegoulia 2002]. Larger S_q and S_{dr} roughness values and a smaller S_{cl} roughness value at sub-nanometer scale have previously been shown to increase the *S. aureus* adhesion [Webb 2013]. In this study, the comparison between these small scale roughness values of the PS and ABS phases (Table 3) gave a similar trend for the bacterial adhesion. The Lewis acid-base characteristics of ABS may contribute to the attractive interactions with bipolar materials such as *S. aureus* bacteria [Li 2004, van Oss 1987]. In comparison to ABS, glass shows similar surface properties (surface energy and roughness) and bacterial adhesion.

Avidin-coated latex surfaces affected *S. aureus* adhesion in a different way, depending on the coating composition. The slightly enhanced bacterial adhesion to avidin on the ABS surface and the two-component coating with 85 % surface coverage of PS, compared to the avidin-free latex surfaces, possibly originated from the specific interaction between *S. aureus* and avidin [Korpela 1984]. Contrary to the aforementioned latex coatings, the pre-adsorbed avidin on two-component latex with 55 % surface

coverage of PS reduced the adhesion of *S. aureus* to the same level as PDMS that is known for its biomaterial repellency (see also section 6.3.1.). The decreased contact area probably leads to the suppressed specific interactions. In this case, the repulsion caused by the hydrophilic and hydrated avidin molecules could dominate the interaction, leading to suppressed bacterial adhesion. Considering that *S. aureus* biofilms treated with a high concentration of penicillin G for 24 h showed a bacterial viable count reduction of 1 log (CFU/cm^2), the suppressed bacterial adhesion caused by nano-texturing and preadsorbed avidin is relatively significant [Manner 2013].

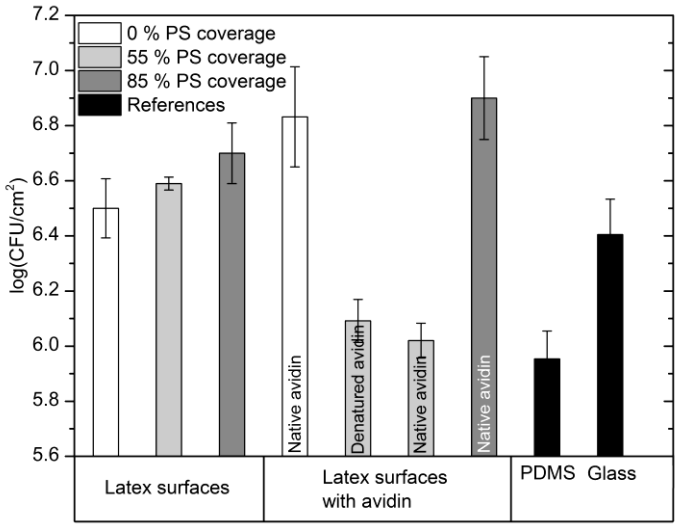

Figure 27. The effect of the substrate on adhesion of *S. aureus*.

In order to enable a fast and high-throughput manner of using the printed paper-based cell study arrays, as e.g. screening assays, the application of a *S. aureus* suspension was demonstrated by a simple pipetting procedure. The micrographs and AFM topographs show that the two-component latex surface supported adhesion of bacteria more uniformly than the corresponding coating with preadsorbed avidin (Figure 28). On the avidin-coated latex surface, a larger variation in the coverage of *S. aureus* was observed.

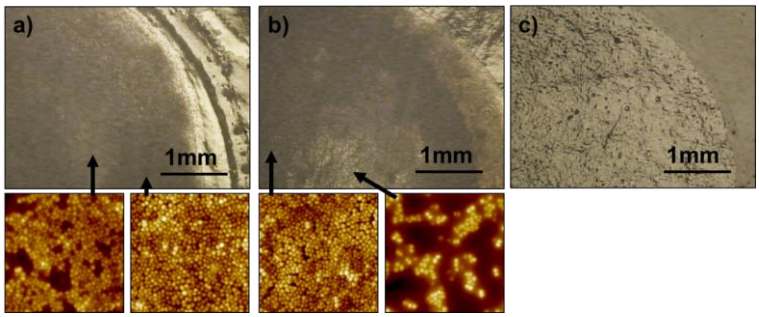

Figure 28. Optical micrographs of the test areas of cell study arrays with *S. aureus* applied to the surface by the drop deposition method a) on two-component latex and b) on avidin-coated two-component latex. An empty 2D-well is shown as a reference in c). AFM topographs with low and high bacterial density are shown below the micrographs. The size of the AFM topographs is 25 µm × 25 µm. Paper 3.

7. CONCLUSIONS AND OUTLOOK

Protein adsorption and cellular adhesion to the surface of different coated paper substrates were studied, with the aim of developing a paper-based roll-to-roll printable test platform for e.g. immunoassay applications and cell studies. The surface properties of the substrates were studied and attributed to protein adsorption and cell growth.

The latex coatings were modified by treating the pristine surfaces with short-wave IR irradiation and by changing the composition of the binary latex coatings, which enabled the tailoring of the surface properties. Randomly distributed nanopatterned topography with two distinct height levels of hydrophobic polystyrene (PS) and hydrophilic acrylonitrile butadiene styrene (ABS) was formed when the pristine two-component latex surface was IR treated. The effective surface area of the hydrophobic PS component increased linearly with increasing fraction of PS in the latex blend up to PS:ABS = 60:40 wt%.

Protein adsorption was more pronounced on the hydrophobic phase of the IR-treated two-component latex coating due to the

hydrophobic interactions. As a result, adsorption of proteins resulted in a patterned structure, i.e. a higher concentration of protein on PS compared to ABS. On the pristine surface, similar directed protein adsorption did not occur due to the electrostatic repulsion caused by the surfactant molecules. Avidin adsorbed to both of the latex components, but adsorption to hydrophobic PS was more pronounced, which was attributed to the hydrophobic interactions. Also the orientation of the avidin molecules was suggested to have an effect on the adsorption. On ABS, avidin showed a better specific binding activity to biotin, probably due to the better retained conformation on the hydrophilic surface and accessibility of the binding sites, whereas the surface-induced conformational changes may have reduced the binding activity on the hydrophobic PS phase. The higher packing density on PS may have increased the steric hindrance effect.

Cell adhesion and growth could be directed to the test areas of the paper-based cell study platform by printing a patterned structure of PDMS over the paper substrate. Four different paper substrates were evaluated as cell study substrates by studying the growth of ARPE-19 cells. A suitable combination of physico-chemical surface properties such as roughness and surface energy was important for a successful growth of ARPE-19 cells. A two-component latex coating was found to be a good support for the ARPE-19 cells and *S. aureus* bacteria. Bacterial adhesion to the latex coating was increased with the hydrophobicity of the surface and, additionally, the specific interactions between avidin and *S. aureus* enhanced the adhesion to the surface with a sufficiently low void volume (high contact area). Pre-adsorbed avidin inhibited significantly the bacterial adhesion on the two-component latex surface with a high value of void volume. This finding may open up a way for the development of new types of antimicrobial surfaces.

Up-scalable fabrication methods are a prerequisite when developing new test platforms for high-throughput screening of biomaterials. In this study, the methods used for coating the paper substrates with latex are all roll-to-roll compatible, enabling low-cost and fast preparation of the described test platforms. The applicability of the printing and roll-to-roll processes for the transfer of proteins and cells was shown. Ink-jet printed

streptavidin was showed to retain its activity and the ARPE-19 and HepG2 cells were viable after screen-printing.

Since the used test platform enables protein adsorption and cell adhesion, it could also be used e.g. in immunoassays using avidin-biotin chemistry, screening assays for cytotoxicity testing and biofilm studies. The usability of the test platform for cell studies could be improved by using transparent substrates with the developed latex coating material which would enable the use of optical techniques for e.g. cell viability analyses. A systematic study of surface conditioning by chemical and biochemical substances that are present in the cell medium is also needed for further development of the test platform. The study on the mass, orientation and conformation of e.g. cell adhesive proteins adsorbed from multi-protein solutions would provide important information for understanding the cell-latex surface interactions. In addition, the anti-microbial properties related to protein-coated surfaces would be an interesting topic for further studies.

8. ACKNOWLEDGEMENTS

I acknowledge professor Jouko Peltonen for the possibility to work in his group and accomplish this PhD thesis at the Laboratory of Physical Chemistry at Åbo Akademi University. I appreciate deeply his valuable supervision and the chance to work in a multi-disciplinary way with several different research areas.

I am grateful to adjunct professor Petri Ihalainen for his important impact to this study. He has always provided his broad knowledge and all his effort to help me go forward in my work. I appreciate Petri's overall genuine attitude and his efficient way to steer a research team.

I acknowledge all of the members of my research group and my co-authors for the very good collaboration. I feel privileged to have learned a lot from the experts of different research interests through the shared projects.

Every single colleague at FyKe and PaF throughout the years is thanked for creating a unique atmosphere to memorize in the future. Especially, I want to thank Anni for sharing all these years at Åbo Akademi. Christina and Kenneth are warmly acknowledged for their helpfulness in so many questions. My special thanks go to all of my great roommates for the numerous enlightening discussions about work and life.

My warmest thanks go to my family, my family-in-law and friends. Dearest Christoffer and Vilmer, you set everything in the right perspective.

REFERENCES

Albers WM, Pelto JM, Suspene C, Määttä JA, Yassar A, Hytönen VP, Vikholm-Lundin IM, Tappura K, Structural and Functional Characteristics of Chimeric Avidins Physically Adsorbed onto Functionalized Polythiophene Thin Films, *Acs Applied Materials & Interfaces,* 4 (2012) 4067.

ATCC, American Type Culture Collection, http://www.lgcstandards-atcc.org/Products/All/HB-8065.aspx, (2014).

Atkins P, de Paula J, Atkins´ Physical Chemistry, Oxford University Press, Oxford New York (2010).

Aydin D, Hirschfeld-Warneken V, Louban I, Spatz J, Micro- and Nanopatterning of Active Biomolecules and Cells, in: Grandin M, Textor M (Eds.), Intelligent Surfaces in Biotechnology, John Wiley & Sons, Inc., Hoboken, New Yersey, USA (2012) 291.

Backfolk K, Andersson C, Peltonen J, Association between a sodium salt of a linear dodecylbenzene sulphonate and a non-ionic fatty alcohol ethoxylate surfactant during film formation of styrene/butadiene latex, *Colloids and Surfaces A-Physicochemical and Engineering Aspects,* 291 (2006) 38.

Baharloo B, Textor M, Brunette DM, Substratum roughness alters the growth, area, and focal adhesions of epithelial cells, and their proximity to titanium surfaces, *Journal of Biomedical Materials Research Part A,* 74A (2005) 12.

Banerjee I, Pangule RC, Kane RS, Antifouling Coatings: Recent Developments in the Design of Surfaces That Prevent Fouling by Proteins, Bacteria, and Marine Organisms, *Adv Mater,* 23 (2011) 690.

Belegrinou S, Mannelli I, Lisboa P, Bretagnol F, Valsesia A, Ceccone G, Colpo P, Rauscher H, Rossi F, pH-dependent immobilization of proteins on surfaces functionalized by plasma-enhanced chemical vapor deposition of poly(acrylic acid)- and poly(ethylene oxide)-like films, *Langmuir,* 24 (2008) 7251.

Bhattacharya M, Malinen M, Lauren P, Lou Y-R, Kuisma S, Kanninen L, Lille M, Corlu A, Guguen-Guillouzo C, Ikkala O, Laukkanen A, Urtti A, Yliperttula M, Nanofibrillar cellulose hydrogel promotes three-dimensional liver cell culture, *Journal of Controlled Release*, 164 (2012) 291.

Bingen P, Wang G, Steinmetz NF, Rodahl M, Richter RP, Solvation Effects in the Quartz Crystal Microbalance with Dissipation Monitoring Response to Biomolecular Adsorption. A Phenomenological Approach, *Anal.Chem.,* 80 (2008) 8880.

Binnig G, Quate CF, Gerber C, Atomic Force Microscope, *Phys.Rev.Lett.,* 56 (1986) 930.

Blateyron F, The Areal Field Parameters, in: Leach R (Ed.), Characterisation of Areal Surface Texture, Springer-Verlag Berlin Heidelberg (2013) 15.

Blunt L, Jiang X, Numerical Parameters for Characterisation of Topography, in: Advanced Techniques for Assessment Surface Topography: Development of a Basis for 3D Surface Texture Standards "Surfstand", Kogan Page Science (2003) 17.

Bollström R, Määttänen A, Tobjörk D, Ihalainen P, Kaihovirta N, Österbacka R, Peltonen J, Toivakka M, A multilayer coated fiber-based substrate suitable for printed functionality, *Organic Electronics,* 10 (2009) 1020.

Bollström R, Tuorninen M, Määttänen A, Peltonen J, Toivakka M, Top layer coatability on barrier coatings, *Progress in Organic Coatings,* 73 (2012) 26.

Bordwell FG, Cornforth FJ, Application of Hammett Equation to Equilibrium Acidities of Meta-Substituted and Para-Substituted Acetophenones, *J.Org.Chem.,* 43 (1978) 1763.

Briggs D, Seah M, Practical surface analysis: Auger and X-Ray Photoelectron Spectroscopy, John Wiley & Sons (1994) 674.

Calvert P, Printing cells, *Science,* 318 (2007) 208.

Carter DC, He XM, Munson SH, Twigg PD, Gernert KM, Broom MB, Miller TY, 3-Dimensional Structure of Human-Serum Albumin, *Science,* 244 (1989) 1195.

Chang CC, Boland ED, Williams SK, Hoying JB, Direct-write bioprinting three-dimensional biohybrid systems for future regenerative therapies, *Journal of Biomedical Materials Research Part B-Applied Biomaterials,* 98B (2011) 160.

Chapman RG, Ostuni E, Takayama S, Holmlin RE, Yan L, Whitesides GM, Surveying for surfaces that resist the adsorption of proteins, *J.Am.Chem.Soc.,* 122 (2000) 8303.

Chibowski E, Thin layer wicking - Methods for the determination of acid-base free energies of interaction, in: Mittal K (Ed.), Acid-Base Interactions: Relevance to Adhesion Science and Technology, VSP BV, The Netherlands (2000) 419.

Curtis A, The Competitive Effects of Serum-Proteins on Cell-Adhesion, *J.Cell.Sci.,* 71 (1984) 17.

Czichos H, Saito T, Smith L, Springer Handbook of Materials Measurement Methods, Springer Science+Business Media (2006) 255.

De Haenen J, Scholte B, Coated printing sheet and process for making same, WO 2004030917 A1 (2004).

Dee K, Puleo D, Bizios R, Protein-Surface Interactions, in: Bizios R, Dee K, Puleo D (Eds.), An Introduction to Tissue-Biomaterial Interactions, Wiley & Sons, Inc., USA (2002).

Derda R, Tang SKY, Laromaine A, Mosadegh B, Hong E, Mwangi M, Mammoto A, Ingber DE, Whitesides GM, Multizone paper platform for 3-D cell cultures. *PLoS One*, 6 (2011) 18940.

Diamandis EP, Christopoulos TK, The Biotin-(Strept)Avidin System: Principles and Applications in Biotechnology, *Clin. Chem.*, 37 (1991) 625.

Donlan RM, Costerton JW, Biofilms: Survival mechanisms of clinically relevant microorganisms, *Clin.Microbiol.Rev.,* 15 (2002) 167.

D'Sa RA, Burke GA, Meenan BJ, Protein adhesion and cell response on atmospheric pressure dielectric barrier discharge-modified polymer surfaces, *Acta Biomaterialia,* 6 (2010) 2609.

Dunn KC, Aotaki-Keen AE, Putkey FR, Hjelmeland LM, ARPE-19, a human retinal pigment epithelial cell line with differentiated properties, *Exp.Eye Res.,* 62 (1996) 155.

Dupont-Filliard A, Billon M, Bidan G, Guillerez S, Investigation by QCM of the specific and nonspecific avidin interaction onto a biotinylated polypyrrole film, *Electroanalysis,* 16 (2004) 667.

Ekman D, Björklund ÅK, Frey-Skött J, Elofsson A, Multi-domain proteins in the three kingdoms of life: Orphan domains and other unassigned regions, *J. Mol. Biol.*, 348 (2005) 231.

El-Aasser M, Methods of Latex Cleaning, in: Poehlein G, Ottewill R, Goodwin J (Eds.), Science and Technology of Polymer Colloids, Nato ASI Series (1983) 422.

Feinberg AW, Wilkerson WR, Seegert CA, Gibson AL, Hoipkemeier-Wilson L, Brennan AB, Systematic variation of microtopography, surface chemistry and elastic modulus and the state dependent effect on endothelial cell alignment, *Journal of Biomedical Materials Research Part a,* 86A (2008) 522.

Flemming RG, Murphy CJ, Abrams GA, Goodman SL, Nealey PF, Effects of synthetic micro- and nano-structured surfaces on cell behavior, *Biomaterials,* 20 (1999) 573.

Fujihira M, Kelvin probe force microscopy of molecular surfaces, *Annual Review of Materials Science,* 29 (1999) 353.

Garcia R, Perez R, Dynamic atomic force microscopy methods, *Surface Science Reports,* 47 (2002) 197.

Girifalco LA, Good RJ, A Theory for the Estimation of Surface and Interfacial Energies .1. Derivation and Application to Interfacial Tension, *J.Phys.Chem.,* 61 (1957) 904.

Gottenbos B, Busscher HJ, van der Mei HC, Pathogenesis and prevention of biomaterial centered infections, *Journal of Materials Science-Materials in Medicine,* 13 (2002) 717.

Goy-Lopez S, Juarez J, Alatorre-Meda M, Casals E, Puntes VF, Taboada P, Mosquera V, Physicochemical Characteristics of Protein-NP Bioconjugates: The Role of Particle Curvature and Solution Conditions on Human Serum Albumin Conformation and Fibrillogenesis Inhibition, *Langmuir,* 28 (2012) 9113.

Green NM, Avidin. *Adv.Protein Chem.,* 29 (1975) 85.

Green NM, Avidin and Streptavidin, *Meth.Enzymol.,* 184 (1990) 51.

Guillotin B, Guillemot F, Cell patterning technologies for organotypic tissue fabrication, *Trends Biotechnol.,* 29 (2011) 183.

Hardin M, Madler K, Bruker MultiMode V SPM Instruction Manual 004-995-000; 004-995-100, Bruker (2011).

Huang S, Swerdlow H, Caldwell K, Binding of Biotinylated Dna to Streptavidin-Coated Polystyrene Latex, *Anal.Biochem.,* 222 (1994) 441.

Høiby N, Bjarnsholt T, Moser C, Bassi GL, Coenye T, Donelli G, Hall-Stoodley L, Holá V, Imbert C, Kirketerp-Møller K, Lebeaux D, Oliver A, Ullmann AJ, Williams C; ESCMID guideline for the diagnosis and treatment of biofilm infections 2014, *Clin Microbiol Infect.* 21 Suppl 1 (2014) 1.

Ihalainen P, Majumdar H, Viitala T, Törngren B, Näreoja T, Määttänen A, Sarfraz J, Härmä H, Yliperttula M, Österbacka R, Peltonen J, Application of Paper-Supported Printed Gold Electrodes for Impedimetric Immunosensor Development. *Biosensors,* 3 (2013) 1.

Jachimska B, Pajor A, Physico-chemical characterization of bovine serum albumin in solution and as deposited on surfaces, *Bioelectrochemistry,* 87 (2012) 138.

Jeon H, Kang K, Park SA, Kim WD, Paik SS, Lee S-H, Jeong J, Choi D, Generation of Multilayered 3D Structures of HepG2 Cells Using a Bio-printing Technique, *Gut and Liver*, (2016) doi 10.5009/gnl16010.

Jeyachandran YL, Mielezarski E, Rai B, Mielczarski JA, Quantitative and Qualitative Evaluation of Adsorption/Desorption of Bovine Serum Albumin on Hydrophilic and Hydrophobic Surfaces, *Langmuir,* 25 (2009) 11614.

Ji J, Feng LX, Qiu YX, Yu XJ, Stearyl poly(ethylene oxide) grafted surfaces for preferential adsorption of albumin Part 2. The effect of molecular mobility on protein adsorption, *Polymer,* 41 (2000) 3713.

Kaelble DH, Moacanin J, A surface energy analysis of bioadhesion, *Polymer,* 18 (1977) 475.

Kamiya Y, Yamazaki K, Ogino T, Protein adsorption to graphene surfaces controlled by chemical modification of the substrate surfaces, *J.Colloid Interface Sci.,* 431 (2014) 77.

Kastritis PL, Bonvin AMJJ, On the binding affinity of macromolecular interactions: daring to ask why proteins interact, *Journal of the Royal Society Interface,* 10 (2013).

Katsikogianni M, Missirlis YF, Concise review of mechanisms of bacterial adhesion to biomaterials and of techniques used in estimating bacteria-material interactions. *European cells & materials,* 8 (2004) 37.

Keogh JR, Eaton JW, Albumin-Binding Surfaces for Biomaterials, *J.Lab.Clin.Med.,* 124 (1994) 537.

Kibel M, Surface Analysis Methods in Materials Science, in: O´Connor D, Sexton B, Smart R (Eds.), Springer-Verlag Berlin Heidelberg (2003) 175.

Kidoaki S, Matsuda T, Adhesion forces of the blood plasma proteins on self-assembled monolayer surfaces of alkanethiolates with different functional groups measured by an atomic force microscope, *Langmuir,* 15 (1999) 7639.

Kiedrowski MR, Horswill AR, New approaches for treating staphylococcal biofilm infections, *Antimicrobial Therapeutics Reviews: Antibiotics that Target the Ribosome,* 1241 (2011) 104.

Kim S-H, Lee HR, Yub SJ, Han M-E, Lee DY, Kim SY, Ahn H-J, Hydrogel-laden paper scaffold system for origami-based tissue engineering, *PNAS*, 112 (2015) 15426.

Kowalczynska HM, Nowak-Wyrzykowska M, Kołos R, Dobkowski J, Kaminski J, Semiquantitative evaluation of fibronectin adsorption on unmodified and sulfonated polystyrene, as related to cell adhesion, *J. Biomed. Mater. Res. A,* 87 A (2008) 944

Kumar N, Parajuli O, Gupta A, Hahm J, Elucidation of protein adsorption behavior on polymeric surfaces: Toward high-density, high-payload protein templates, *Langmuir,* 24 (2008) 2688.

Li BK, Logan BE, Bacterial adhesion to glass and metal-oxide surfaces, *Colloids and Surfaces B-Biointerfaces,* 36 (2004) 81.

Lim J, Byun S, Chung S, Park T, Seo J, Joo C, Chung H, Cho D, Retinal pigment epithelial cell behavior is modulated by alterations in focal cell-substrate contacts, *Invest.Ophthalmol.Vis.Sci.,* 45 (2004) 4210.

Lindman S, Lynch I, Thulin E, Nilsson H, Dawson KA, Linse S, Systematic investigation of the thermodynamics of HSA adsorption to N-iso-propylacrylamide/N-tert-butylacrylamide copolymer nanoparticles. Effects of particle size and hydrophobicity, *Nano Letters,* 7 (2007) 914.

Lister JL, Horswill AR, Staphylococcus aureus biofilms: recent developments in biofilm dispersal, *Frontiers in Cellular and Infection Microbiology,* 4 (2014).

Liu D, Wang T, Keddie JL, Protein Nanopatterning on Self-Organized Poly(styrene-b-isoprene) Thin Film Templates, *Langmuir,* 25 (2009) 4526.

Livnah O, Bayer EA, Wilchek M, Sussman JL, 3-Dimensional Structures of Avidin and the Avidin-Biotin Complex, *Proc. Natl. Acad. Sci. U.S.A.,* 90 (1993) 5076.

Löberg J, Mattisson I, Hansson S, Ahlberg E, Characterisation of Titanium Dental Implants I: Critical Assessment of Surface Roughness Parameters, *The Open Biomaterials Journal,* 2 (2010) 18.

Manner S, Skogman M, Goeres D, Vuorela P, Fallarero A, Systematic Exploration of Natural and Synthetic Flavonoids for the Inhibition of Staphylococcus aureus Biofilms, *International Journal of Molecular Sciences,* 14 (2013) 19434.

Martins NTC, Freire CSR, Neto CP, Silvestre AJD, Causio J, Baldi G, Sadocco P, Trindade T, Antibacterial paper based on composite coatings of nanofibrillated cellulose and ZnO, *Colloids and Surfaces A-Physicochemical and Engineering Aspects*, 417 (2013) 111

Marmur A, Solid-Surface Characterization by Wetting, *Annual Review of Materials Research,* 39 (2009) 473.

Merrett K, Cornelius RM, McClung WG, Unsworth LD, Sheardown H, Surface analysis methods for characterizing polymeric biomaterials, *Journal of Biomaterials Science-Polymer Edition,* 13 (2002) 593.

Mironov V, Trusk T, Kasyanov V, Little S, Swaja R, Markwald R, Biofabrication: a 21st century manufacturing paradigm, *Biofabrication,* 1 (2009).

Misawa N, Yamamura S, Yong-Hoon K, Tero R, Nonogaki Y, Urisu T, Orientation of avidin molecules immobilized on COOH-modified SiO2/Si(100) surfaces, *Chem. Phys. Lett.*, 419 (2006) 86.

Morga M, Adamczyk Z, Goedrich S, Ocwieja M, Papastavrou G, Monolayers of poly-L-lysine on mica - Electrokinetic characteristics, *J.Colloid Interface Sci.,* 456 (2015) 116.

Müller R, Gröger G, Hiller K, Schmalz G, Ruhl S, Fluorescence-based bacterial overlay method for simultaneous in situ quantification of surface-attached bacteria, *Appl.Environ.Microbiol.,* 73 (2007) 2653.

Myers D, Surfaces, Interfaces, and Colloids, John Wiley & Sons, Inc., USA (1999) 83.

Määttänen A, Fors D, Wang S, Valtakari D, Ihalainen P, Peltonen J, Paper-based planar reaction arrays for printed diagnostics, *Sensors Actuators B: Chem.,* 160 (2011) 1404.Ng K, Gao B, Yong K, Li Y, Shi M, Zhao X, Li Z, Zhang X, Pingguan-Murphy B, Yang H, Xu F, Paper-based cell culture platform and its emerging biomedical applications, *Mater. Today*, (2016) http://dx.doi.org/10.1016/j.mattod.2016.07.001.

Norde W, Anusiem ACI, Adsorption, desorption and re-adsorption of proteins on solid surfaces, *Colloids Surf.*, 66 (1992) 73.

Ntmdt W, www.ntmdt.com/spm-basics/view/effect-tip-radius-cone-angle, (2016).

Oja T, Blomqvist B, Buckingham-Meyer K, Goeres D, Vuorela P, Fallarero A, Revisiting an agar-based plate method: What the static biofilm method can offer for biofilm research, *J.Microbiol.Methods,* 107 (2014) 157.

Oliver AE, Ngassam V, Dang P, Sanii B, Wu H, Yee CK, Yeh Y, Parikh AN, Cell Attachment Behavior on Solid and Fluid Substrates Exhibiting Spatial Patterns of Physical Properties, *Langmuir,* 25 (2009) 6992.

Otsuka H, Nagasaki Y, Kataoka K, Dynamic wettability study on the functionalized PEGylated layer on a polylactide surface constructed by the coating of aldehyde-ended poly(ethylene glycol) (PEG)/polylactide (PLA) block copolymer, *Science and Technology of Advanced Materials,* 1 (2000) 21.

Otsuka H, Nagasaki Y, Kataoka K, Characterization of aldehyde-PEG tethered surfaces: Influence of PEG chain length on the specific biorecognition, *Langmuir,* 20 (2004) 11285.

Owens D, and Wendt R, Estimation of the surface free energy of polymers, *J. Appl. Polym. Sci.,* 13 (1969) 1741.

Pankov R, Yamada KM, Fibronectin at a glance, *J.Cell.Sci.,* 115 (2002) 3861.

Parolo C, Merkoçi A, Paper-based nanobiosensors for diagnostics, *Chem. Soc. Rev.*, 42 (2013) 450.

Pelton R, Bioactive paper provides a low-cost platform for diagnostics, *Trac-Trends Anal.Chem.,* 28 (2009) 925.

Peltonen J, Järn M, Areva S, Lindén M, Rosenholm J, Topographical parameters for specifying a three-dimensional surface, *Langmuir,* 20 (2004) 9428.

Plow EF, Haas TK, Zhang L, Loftus J, Smith JW, Ligand binding to integrins, *J.Biol.Chem.,* 275 (2000) 21785.

Ray S, Steven RT, Green FM, Hook F, Taskinen B, Hytonen VP, Shard AG, Neutralized Chimeric Avidin Binding at a Reference Biosensor Surface, *Langmuir,* 31 (2015) 1921.

Redey S, Nardin M, Bernache-Assolant D, Rey C, Delannoy P, Sedel L, Marie P, Behavior of human osteoblastic cells on stoichiometric hydroxyapatite and type A carbonate apatite: Role of surface energy, *J.Biomed.Mater.Res.,* 50 (2000) 353.

Ribeiro C, Panadero JA, Sencadas V, Lanceros-Méndez L, Tamaño MN, Moratal D, Salmerón-Sánchez M, Gómez Ribelles JL, Fibronectin adsorption and cell response on electroactive poly(vinylidene fluoride) films, *Biomed. Mater.*, 7 (2012) 1.

Riedel M, Muller B, Wintermantel E, Protein adsorption and monocyte activation on germanium nanopyramids, *Biomaterials,* 22 (2001) 2307.

Rockwell GP, Lohstreter LB, Dahn JR, Fibrinogen and albumin adsorption on titanium nanoroughness gradients, *Colloids and Surfaces B-Biointerfaces,* 91 (2012) 90.

Rodahl M, Höök F, Krozer A, Brzezinski P, Kasemo B, Quartz-Crystal Microbalance Setup for Frequency and Q-Factor Measurements in Gaseous and Liquid Environments, *Rev.Sci.Instrum.,* 66 (1995) 3924.

Rodahl M, Kasemo B, A simple setup to simultaneously measure the resonant frequency and the absolute dissipation factor of a quartz crystal microbalance, *Rev.Sci.Instrum.,* 67 (1996) 3238.

Rodahl M, Höök F, Fredriksson C, Keller CA, Krozer A, Brzezinski P, Voinova M, Kasemo B, Simultaneous frequency and dissipation factor QCM measurements of biomolecular adsorption and cell adhesion, *Faraday Discuss.,* 107 (1997) 229.

Sahin O, Time-varying tip-sample force measurements and steady-state dynamics in tapping-mode atomic force microscopy, *Physical Review B,* 77 (2008).

Sahin O, Erina N, High-resolution and large dynamic range nanomechanical mapping in tapping-mode atomic force microscopy, *Nanotechnology,* 19 (2008).

Sarfraz J, Määttänen A, Ihalainen P, Keppeler M, Lindén M, Peltonen J, Printed copper acetate based H2S sensor on paper substrate, *Sensors and Actuators B-Chemical,* 173 (2012) 868.

Satriano C, Carnazza S, Guglielmino S, Marletta G, Surface free energy and cell attachment onto ion-beam irradiated polymer surfaces, *Nuclear Instruments & Methods in Physics Research Section B-Beam Interactions with Materials and Atoms,* 208 (2003) 287.

Sauerbrey G, Verwendung Von Schwingquarzen Zur Wagung Dunner Schichten Und Zur Mikrowagung, *Zeitschrift Fur Physik,* 155 (1959) 206.

Scott T, Eagleson M, Concise Encyclopedia: Biochemistry, Walter de Gruyer, New York (1988).

Seigel RR, Harder P, Dahint R, Grunze M, Josse F, Mrksich M, Whitesides GM, On-line detection of nonspecific protein adsorption at artificial surfaces. *Anal.Chem.,* 69 (1997) 3321.

Sjöberg B, Eriksson M, Österlund E, Pap S, Österlund K, Solution Structure of Human-Plasma Fibronectin as a Function of Nacl Concentration Determined by Small-Angle X-Ray-Scattering, *European Biophysics Journal with Biophysics Letters,* 17 (1989) 5.

Somorjai G, Li Y, Introduction to Surface Chemistry and Catalysis, John Wiley & Sons, Inc., Hoboken, New Jersey (2010).

Steward PA, Hearn J, Wilkinson MC, An overview of polymer latex film formation and properties, *Adv.Colloid Interface Sci.,* 86 (2000) 195.

Sutherland DS, Broberg M, Nygren H, Kasemo B, Influence of nanoscale surface topography and chemistry on the functional behaviour of an adsorbed model macromolecule, *Macromolecular Bioscience,* 1 (2001) 270.

Taylor KE, van den Berg CW, Structural and functional comparison of native pentameric, denatured monomeric and biotinylated C-reactive protein, *Immunology,* 120 (2007) 404.

Tegoulia VA, Cooper SL, Staphylococcus aureus adhesion to self-assembled monolayers: effect of surface chemistry and fibrinogen presence, *Colloids and Surfaces B-Biointerfaces,* 24 (2002) 217.

Teixeira A, Abrams G, Bertics P, Murphy C, Nealey P, Epithelial contact guidance on well-defined micro- and nanostructured substrates, *J.Cell.Sci.,* 116 (2003) 1881.

Tran ATT, James BJ, A study the interaction forces between the bovine serum albumin protein and montmorillonite surface, *Colloids and Surfaces A-Physicochemical and Engineering Aspects,* 414 (2012) 104.

Tsapikouni TS, Missirlis YF, Protein-material interactions: From micro-to-nano scale, *Materials Science and Engineering B-Advanced Functional Solid-State Materials,* 152 (2008) 2.

Valle-Delgado JJ, Molina-Bolivar JA, Galisteo-Gonzalez F, Galvez-Ruiz MJ, Evidence of hydration forces between proteins, *Current Opinion in Colloid & Interface Science,* 16 (2011) 572.

van den Hul, H. J., Vanderhoff JW, Inferences on Mechanism of Emulsion Polymerisation of Styrene from Characterisation of Polymer End-Groups, *Chemical and Process Engineering,* 51 (1970) 89.

van Oss C, Chaudhury M, Good R, Interfacial Lifshitz-van der Waals and Polar Interactions in Macroscopic
Systems, *Chemical Reviews, Chem. Rev.,* 6 (1988) 927.

van Oss CJ, Acid—base interfacial interactions in aqueous media, *Colloids Surf.Physicochem.Eng.Aspects,* 78 (1993) 1.

van Oss CJ, Long-range and short-range mechanisms of hydrophobic attraction and hydrophilic repulsion in specific and aspecific interactions, *Journal of Molecular Recognition,* 16 (2003 a) 177.

van Oss C, Giese R, Bronson P, Docoslis A, Edwards P, Ruyechan W, Macroscopic-scale surface properties of streptavidin and their influence on aspecific interactions between streptavidin and dissolved biopolymers, *Colloids and Surfaces B-Biointerfaces,* 30 (2003 b) 25.

van Oss CJ, Chaudhury MK, Good RJ, Monopolar Surfaces, *Adv.Colloid Interface Sci.,* 28 (1987) 35.

Vikholm-Lundin I, Auer S, Paakkunainen M, Määttä JAE, Munter T, Leppiniemi J, Hytönen VP, Tappura K, Cysteine-tagged chimeric avidin

forms high binding capacity layers directly on gold, *Sensors and Actuators B-Chemical,* 171 (2012) 440.

Vogler E, Structure and reactivity of water at biomaterial surfaces, *Adv.Colloid Interface Sci.,* 74 (1998) 69.

Vogler EA, Protein adsorption in three dimensions, *Biomaterials,* 33 (2012) 1201.

Vogt BD, Lin EK, Wu WL, White CC, Effect of film thickness on the validity of the Sauerbrey equation for hydrated polyelectrolyte films, *J Phys Chem B,* 108 (2004) 12685.

Wang K, Zhou C, Hong Y, Zhang X, A review of protein adsorption on bioceramics, *Interface Focus,* 2 (2012) 259.

Webb HK, Boshkovikj V, Fluke CJ, Truong VK, Hasan J, Baulin VA, Lapovoke R, Estrin Y, Crawford RJ, Ivanova EP, Bacterial attachment on sub-nanometrically smooth titanium substrata, *Biofouling,* 29 (2013) 163.

Wei Q, Becherer T, Angioletti-Uberti S, Dzubiella J, Wischke C, Neffe AT, Lendlein A, Ballauff M, Haag R, Protein Interactions with Polymer Coatings and Biomaterials, *Angewandte Chemie-International Edition,* 53 (2014) 8004.

Wenzel R, Resistance of Solid Surfaces to Wetting by Water, *Industrial & Engineering Chemistry, Ind. Eng. Chem.,* 28 (1936) 988.

Wilchek M, Bayer EA, The Avidin Biotin Complex in Bioanalytical Applications, *Anal.Biochem.,* 171 (1988) 1.

Williams E, Janmey P, Ferry J, Mosher D, Conformational States of Fibronectin - Effects of Ph, Ionic-Strength, and Collagen Binding, *J.Biol.Chem.,* 257 (1982) 4973.

Williams RA, Blanch HW, Covalent Immobilization of Protein Monolayers for Biosensor Applications, *Biosens.Bioelectron.,* 9 (1994) 159.

Young T, An Essay of the Cohesion of Fluids, *Philosophical Transactions of the Royal Society A, Phil. Trans. R. Soc. Lond. A,* (1804) 65.

Young TJ, Monclus MA, Burnett TL, Broughton WR, Ogin SL, Smith PA, The use of the PeakForce (TM) quantitative nanomechanical mapping AFM-based method for high-resolution Young's modulus measurement of polymers, *Meas Sci Technol,* 22 (2011).

Zenkiewicz M, Comparative study on the surface free energy of a solid calculated by different methods, *Polym.Test.,* 26 (2007) 14.

Zhong Q, Inniss D, Kjoller K, Elings VB, Fractured Polymer Silica Fiber Surface Studied by Tapping Mode Atomic-Force Microscopy, *Surf.Sci.,* 290 (1993) L688.

Zocchi A, Jobe AM, Neuhaus JM, Ward TR, Expression and purification of a recombinant avidin with a lowered isoelectric point in Pichia pastoris, *Protein Expr.Purif.,* 32 (2003) 167.

Österlund E, The Secondary Structure of Human-Plasma Fibronectin - Conformational-Changes Induced by Acidic Ph and Elevated-Temperatures - a Circular Dichroic Study, *Biochim.Biophys.Acta,* 955 (1988) 330.

ISBN 978-952-12-3476-7